

1 Matrix-associated extracellular vesicles modulate smooth muscle cell

2 adhesion and directionality by presenting collagen VI.

3 Alexander Kapustin^{1*}, Sofia Serena Tsakali¹, Meredith Whitehead¹, George Chennel², Meng-Ying
4 Wu^{1,3}, Chris Molenaar¹, Anton Kutikhin⁴, Yimeng Chen¹, Sadia Ahmad¹, Leo Bogdanov⁴, Maxim
5 Sinitsky³, Kseniya Rubina⁵, Aled Clayton⁶, Frederik J Verweij⁷, Dirk Michiel Pegtel⁸, Simona Zingaro⁹,
6 Arseniy Lobov¹⁰, Bozhana Zainullina¹¹, Dylan Owen¹², Maddy Parsons⁹, Richard E. Cheney¹³, Derek
7 Warren¹⁴, Martin James Humphries¹⁵, Thomas Iskratsch¹⁶, Mark Holt⁸, and Catherine M Shanahan^{1*}

8 ¹School of Cardiovascular and Metabolic Medicine & Sciences, James Black Centre, King's College
9 London, 125 Coldharbour Lane, London, SE5 9NU, UK, Tel. 020 7848 5221, FAX 020 7848 5193,

¹⁰ Wohl Cellular Imaging Centre, King's College London, 5 Cutcombe Road, London, SE5 9NU

11 ³Department of Urology, The Third Affiliated Hospital of Soochow University, Changzhou, Jiangsu,
12 China, 213003

13 ⁴Laboratory for Molecular, Translational and Digital Medicine, Research Institute for Complex Issues
14 of Cardiovascular Diseases, 6 Sosnovy Boulevard, Kemerovo, 650002, Russian Federation

15 ⁵Laboratory of Morphogenesis and Tissue Reparation, Faculty of Medicine, Lomonosov Moscow
16 State University, Lomonosovsky av. 27-1, Moscow, 119991, Russia, tel/fax +74959329904

⁶Tissue Microenvironment Research Group, Division of Cancer & Genetics, School of Medicine, Cardiff University, Tenovus Building, Cardiff, UK, CF14 2XN

19 ⁷Division of Cell Biology, Neurobiology & Biophysics, Utrecht University, Padualaan 8, 3584 CH

20 Utrecht, The Netherlands

⁸Amsterdam UMC, Location Vrije Universiteit Amsterdam, Department of Pathology, Cancer Center Amsterdam, De Boelelaan 1117, Amsterdam, The Netherlands.

²³ Randall Centre for Cell and Molecular Biophysics, School of Basic and Medical Biosciences, King's College London, New Hunt's House, Cade Campana, London, SE1 1HL, UK.

25 ¹⁰Laboratory of Regenerative Biomedicine, Institute of Cytology of the Russian Academy of Sciences
26 47 ul. Kosygin, 1310261, St. Petersburg, Russia

²⁷ ¹¹Centre for Molecular and Cell Technologies, Research Park, St. Petersburg State University, 7/9

²⁹ ¹²Institute of Immunology and Immunotherapy, School of Mathematics and Centre of Membrane

31 ¹³Department of Cell Biology and Physiology, School of Medicine, University of North Carolina at

32 Chapel Hill, Chapel Hill, NC 27593, USA
33 ¹⁴School of Pharmacy, University of East Anglia, Norwich Research Park, Norwich, Norfolk, UK, NR4

³⁵ Wellcome Centre for Cell-Matrix Research, Faculty of Biology, Medicine & Health, Manchester

36 Academic Health Science Centre, University of Manchester, Michael Smith Building, Oxford Road,
37 Manchester, M13 9PT, United Kingdom

1 ¹⁶School of Engineering and Materials Science, Faculty of Science and Engineering, Queen Mary
2 University of London, Engineering Building, Mile End Road, E1 4NS

3

4 * Corresponding authors

5 Email: Alexander.kapustin@kcl.ac.uk

6 Words: small extracellular vesicles, cell adhesion, vascular remodelling

7

8

1 **Abstract**

2 The extracellular matrix (ECM) supports blood vessel architecture and functionality and undergoes
3 active remodelling during vascular repair and atherogenesis. Vascular smooth muscle cells (VSMCs)
4 are essential for vessel repair and, via their secretome, can invade from the vessel media into the
5 intima to mediate ECM remodelling. Accumulation of fibronectin (FN) is a hallmark of early vascular
6 repair and atherosclerosis. Here we show that FN stimulates VSMCs to secrete small extracellular
7 vesicles (sEVs) by activating the $\beta 1$ integrin/FAK/Src pathway as well as Arp2/3-dependent branching
8 of the actin cytoskeleton. We found that sEVs are trapped by the ECM *in vitro* and colocalise with FN
9 in symptomatic atherosclerotic plaques *in vivo*. Functionally, ECM-trapped sEVs induced the
10 formation of focal adhesions (FA) with enhanced pulling forces at the cellular periphery preventing
11 cellular spreading and adhesion. Proteomic and GO pathway analysis revealed that VSMC-derived
12 sEVs display a cell adhesion signature and are specifically enriched with collagen VI on the sEV
13 surface. *In vitro* assays identified collagen VI as playing a key role in cell adhesion and invasion
14 directionality. Taken together our data suggests that the accumulation of FN is a key early event in
15 vessel repair acting to promote secretion of collagen VI enriched sEVs by VSMCs. These sEVs stimulate
16 directional invasion, most likely by triggering peripheral focal adhesion formation and actomyosin
17 contraction to exert sufficient traction force to enable VSMC movement within the complex vascular
18 ECM network.

19

1 **Introduction.**

2 The healthy arterial vasculature is dominated by a highly organised medial extracellular matrix (ECM)
3 containing organised layers of contractile vascular smooth muscle cells (VSMCs). Vascular
4 pathologies such as atherosclerosis are associated with dramatic remodelling of the ECM ultimately
5 leading to plaque rupture and myocardial infarction or stroke¹. Progenitor medial VSMCs are
6 essential for vessel repair and must invade through the ECM to form the protective intimal fibrous
7 cap in the plaque. This process of VSMC invasion actively contributes to ECM remodelling²⁻⁴. The
8 accumulation of liver-derived fibronectin (FN) in the vasculature is an early biomarker of
9 atherosclerotic plaque formation and conditional FN knockout in the liver blocked VSMC invasion
10 and fibrous cap formation in the ApoE mouse model. This suggests that FN is an essential signal for
11 VSMC recruitment and invasion during vascular repair, yet its exact role remains unknown⁵⁻⁷.

12 FN has been shown to play key signalling roles by modulating cellular spreading, adhesion, invasion,
13 differentiation and viability during both developmental and pathological processes⁸. Cell adhesion to
14 FN is primarily mediated by $\alpha 5\beta 1$ integrins and proteoglycans acting together to activate small GTP-
15 binding proteins, Cdc42, Rac1, and Rho which in turn induce branched actin cytoskeletal
16 rearrangements to form cellular membrane protrusions, filopodia and lamellipodia, which are
17 attached to the ECM via transient peripheral focal complexes⁸⁻¹¹. In turn, maturation of focal
18 complexes into focal adhesions (FAs) anchors cytoplasmic actin stress fibers to the ECM and actin
19 polymerisation and actomyosin-mediated contractility generate the traction forces required for cell
20 body locomotion^{12, 13}.

21 Exosome-like small extracellular vesicles (sEVs) are novel, cell-matrix crosstalk entities that decorate
22 the ECM and form “migration paths” for tumour cells by enhancing cell adhesion, motility and
23 directionality¹⁴⁻¹⁷. Mechanistically, sEVs are secreted at the cellular leading edge and promote FA
24 formation by presenting fibronectin (FN)^{14, 15, 18, 19}. In addition, sEVs can stimulate motility of
25 immune cells and *Dictyostelium discoideum* by presenting cytokines and/or generating
26 chemoattractants²⁰⁻²². We recently showed that FN is also enriched in VSMC-derived sEVs but the
27 exact role of sEVs in VSMC migration and invasion within the ECM meshwork environment of the
28 vasculature remains unexplored²³.

29 Here we report that FN in the ECM induces sEV secretion by activating $\beta 1$ integrin/FAK/Src and
30 Arp2/3-dependent actin cytoskeleton assembly. In turn, sEVs are trapped to ECM and these ECM-
31 associated sEVs regulate VSMC invasion directionality in a 3D model. Mechanistically ECM-
32 associated sEVs induced earlier formation of focal adhesions (FA) with enhanced pulling forces at the
33 cell periphery thus switching the leading edge from protrusion activity into contractile mode to
34 enable cell body propulsion. Importantly, we found that the sEV cargo, collagen VI, is
35 indispensable for triggering FA formation and directed cell invasion. We hypothesize that sEV-
36 triggered peripheral FA formation anchors the cellular leading edge and activates cell contraction to
37 exert sufficient force to allow VSMC invasion into the complex ECM fibre meshwork. This novel
38 mechanism opens a unique therapeutic opportunity to target specifically VSMC invasion activity
39 during vascular repair and restenosis.

40

41

1 **Results.**

2 **1. ECM components involved in vessel injury repair stimulate sEV release via $\beta 1$ integrins.**

3 FN is detectable in the vasculature as early as the fatty streak stage and preceding major atherogenic
4 alterations such as neointima formation and it is also a novel marker for symptomatic carotid
5 plaques⁵⁻⁷. Given its presence during early stages of vessel injury we hypothesized that FN may
6 modulate sEV secretion to enable vessel repair. FN is secreted as a monomeric protein forming
7 fibrils upon cellular binding so we compared the effects of monomeric FN with the effects of FN
8 immobilised on tissue culture plates to mimic FN fibrils⁸. Plating VSMCs on immobilised FN
9 increased the release of CD63+/CD81+ sEVs 3.5±0.6 fold whilst addition of soluble FN had no effect
10 on EV secretion as detected by CD63-bead capture assay (Fig 1A). Fibrillar collagen I but not a non-
11 fibrillar laminin also stimulated secretion of CD63+/CD81+ sEVs by VSMCs to the same extent as FN
12 (Fig S1A).

13 We next tested if the native VSMC-derived 3D matrix that contains FN and collagen could modulate
14 sEV secretion²⁴. VSMCs were induced to produce ECM, cells were removed and fresh VSMCs plated
15 onto these 3D matrices. VSMCs acquired an elongated shape (Figs 1B and 1C) which is typical for
16 mesenchymal cells in a 3D environment²⁴ and increased secretion of CD63+/CD81+ sEVs compared
17 to VSMCs plated onto the non-coated plastic (Fig 1D). We observed no changes in the size
18 distribution of sEVs secreted by VSMCs plated either on plastic or FN matrix as detected using
19 Nanoparticle Tracking Analysis (NTA) (Fig 1E). To further characterise the EV populations released
20 western blotting confirmed that sEVs isolated in both conditions were loaded with similar levels of
21 FN and the sEV-specific markers CD63 and Syntenin-1 and lacked the EV-specific marker, α -actinin-4
22 (Fig 1F)²⁵. In addition, treatment of the cells plated onto the matrix with sphingomyelin
23 phosphodiesterase 3 inhibitor (3-O-Methyl-Sphingomyelin, 3-OMS) revealed that CD63+/CD81+ sEV
24 secretion in response to collagen and FN was regulated by sphingomyelin phosphodiesterase 3 (Fig
25 S1B) which regulates sEV generation in multivesicular bodies²⁶. Hence, FN triggers secretion of
26 CD63+/CD81+ sEVs, most likely with a late endosomal origin.

27 Both collagen I and FN are ECM ligands that bind and transduce intracellular signalling via $\beta 1$
28 integrin. Therefore, we explored the effect of $\beta 1$ integrin activating (12G10) or inhibiting antibodies
29 (4B4) on FN-stimulated secretion of CD63+/CD81+ sEVs. Activation of $\beta 1$ integrin using 12G10
30 antibody in VSMCs enhanced the effect of FN on sEV secretion (Fig 1G). Inhibition of $\beta 1$ integrin
31 using the 4B4 antibody blocked CD63+/CD81+ sEV secretion by VSMCs plated on FN (Fig 1G). Next,
32 we tested the role of the $\beta 1$ integrin downstream signalling mediators, FAK and Src²⁷. Blocking these
33 pathways with small inhibitors (FAM14 and PP2, respectively) reduced sEV secretion by cells plated
34 on FN but not on plastic (Figs 1H and 1I). Taken together these data suggest that FN matrices
35 stimulate secretion of CD63+/CD81+ sEVs via the $\beta 1$ integrin signalling pathway.

36

37 **2. FN-induced sEV secretion is modulated by Arp2/3 and formin-dependent actin cytoskeleton
38 remodelling**

39 ECM-induced focal FAs initiate dynamic remodelling of the actin cytoskeleton, a process regulated
40 by the Arp2/3 complex and formins, which have recently been implicated in exosome secretion in
41 lymphocytes and tumor cells²⁸⁻³⁰. So next we tested the contribution of Arp2/3 and formins by using
42 the small molecule inhibitors, CK666 and SMIFH2, respectively^{31, 32}. CK666 reduced sEV secretion
43 both in VSMCs plated on plastic and FN matrix while inhibition of formins using SMIFH2 was only

1 effective on the FN matrix (Figs 2A and 2B)-indicating that formins may be involved in FN-dependent
2 sEV secretion.

3 As regulators of branched actin assembly, the Arp2/3 complex and cortactin are thought to
4 contribute to sEV secretion in tumour cells by mediating MVB intracellular transport and plasma
5 membrane docking^{28, 33}. Therefore, we overexpressed the Arp2/3 subunit, ARPC2-GFP and the F-
6 actin marker, F-tractin-RFP in VSMCs and performed live-cell imaging. As expected, Arp2/3 and F-
7 actin bundles formed a distinct lamellipodia scaffold in the cellular cortex (Fig S2A and
8 Supplementary Video S2). Unexpectedly, we also observed numerous Arp2/3/F-actin positive spots
9 moving through the VSMC cytoplasm that resembled previously described endosome actin tails
10 observed in Xenopus eggs³³ and parasite infected cells where actin comet tails propel parasites via
11 filopodia to neighbouring cells^{34, 35} (Fig S2A, arrow, and Supplementary Video S2). Analysis of the
12 intracellular distribution of Arp2/3 and CD63-positive endosomes in VSMCs showed CD63-MVB
13 propulsion by the F-actin tail in live cells (Fig 2C and Supplementary Video S4). Although these were
14 rare events, possibly due to the short observational time in a single microscopic plane (Fig 2C) we
15 observed numerous F-actin spots in fixed VSMCs that were positive both for F-actin and cortactin
16 indicating that these are branched-actin tails (Fig 2D). Moreover, cortactin/F-actin spots colocalised
17 with CD63+ endosomes and addition of the SMPD3 inhibitor, 3-OMS, induced the appearance of
18 enlarged doughnut-like cortactin/F-actin/CD63 complexes resembling invadopodia-like structures
19 similar to those observed in tumour cells (Fig 2D, arrowheads)¹⁸. To quantify CD63 overlap with the
20 actin tail-like structures, we extracted round-shaped actin structures and calculated the thresholded
21 Manders colocalization coefficient (Fig S2B). We observed overlap between F-actin tails and CD63 as
22 well as close proximity of these markers in fixed VSMCs (Fig S2B). Approximately 50% of the F-actin
23 tails were associated with ~13% of all endosomes ($tM1=0.44\pm0.23$ and $tM2=0.13\pm0.06$,
24 respectively, $N=3$). Addition of 3-OMS enhanced this overlap further ($tM1=0.75\pm0.18$ and
25 $tM2=0.25\pm0.09$) suggesting that Arp2/3-driven branched F-actin tails are involved in CD63+ MVB
26 intracellular transport in VSMCs.

27 Formins and the Arp2/3 complex play a crucial role in the formation of filopodia, a cellular
28 protrusion required for sensing the extracellular environment and cell-ECM interactions³⁶. To test
29 whether MVBs can be delivered to filopodia, we stained VSMCs for Myosin-10 (Myo10)³⁷. We
30 observed no difference between total filopodia number per cell on plastic or FN matrices ($n=18\pm8$
31 and $n=14\pm3$, respectively) however the presence of endogenous CD63+ MVBs along the Myo10-
32 positive filopodia were observed in both conditions (Fig 2E, arrows). Filopodia have been implicated
33 in sEV capture and delivery to endocytosis “hot-spots”³⁸, so next we examined the directionality of
34 CD63+ MVB movement in filopodia by overexpressing Myo10-GFP and CD63-RFP in live VSMCs.
35 Importantly, we observed anterograde MVB transport toward the filopodia tip (Fig 2F and
36 Supplementary Video S2) indicative of MVB secretion.

37 We also attempted to visualise sEV release in filopodia using CD63-pHluorin where fluorescence is
38 only observed upon the fusion of MVBs with the plasma membrane³⁹. Using total internal reflection
39 fluorescence microscopy (TIRF) we observed the typical “burst”-like appearance of sEV secretion at
40 the cell-ECM interface in full agreement with an earlier report showing MVB recruitment to
41 invadopodia-like structures in tumor cells¹⁸ (Fig S2B and Supplementary Video S1). Although we also
42 observed an intense CD63-pHluorin staining along filopodia-like structures we were not able to
43 detect typical “burst”-like events to confirm sEV secretion in filopodia. (Fig S2C and Supplemental
44 Video S1).

1 Taken together these data show that sEV secretion by VSMCs is regulated via Arp2/3 and formin-
2 dependent actin cytoskeleton remodelling. Branched actin tails can potentially contribute to MVB
3 intracellular transport and secretion at the VSMC-ECM interface. Interestingly, CD63+ MVBs can be
4 observed in filopodia-like structures suggesting that sEV secretion can also occur spatially via cellular
5 protrusion-like filopodia but more studies are needed to confirm this hypothesis.

6 **3. sEVs are trapped in the ECM in vitro and in atherosclerotic plaque.**

7 EV trapping in the ECM is a prominent feature of the blood vessel media and intima and EVs become
8 more abundant in the ECM with ageing and disease^{40, 41}. Therefore, we next set out to determine if
9 sEVs that are secreted toward the ECM can be trapped in the native matrix *in vitro*. VSMCs were
10 plated on plastic or FN for 24 h and sEVs were visualised by CD63 immunofluorescence. We
11 observed CD63 puncta in proximity to protrusions at the cell periphery (Fig 3A). These CD63+ sEVs
12 were observed both on the plastic and FN-coated plates suggesting that sEVs can bind to the ECM
13 secreted by VSMCs over the 24h incubation. In agreement with our previous data we also observed
14 CD63+ sEV trapping in the native ECM produced by VSMCs over a 7 day period and their
15 reduction/absence from the matrix when VSMCs were treated with SMPD3 siRNA (Fig 3B)⁴¹.

16 To quantify ECM-trapped sEVs we applied a modified protocol for the sequential extraction of
17 extracellular proteins using salt buffer (0.5M NaCl) to release sEVs which are loosely-attached to
18 ECM via ionic interactions, followed by 4M guanidine HCl buffer (GuHCl) treatment to solubilize
19 strongly-bound sEVs (Fig S3A)⁴². We quantified total sEV and characterised the sEV tetraspanin
20 profile in conditioned media, and the 0.5M NaCl and GuHCl fractions using ExoView. The total
21 particle count showed that EVs are both loosely bound and strongly trapped within the ECM. sEV
22 tetraspanin profiling showed differences between these 3 EV populations. While there was close
23 similarity between the conditioned media and the 0.5M NaCl fraction with high abundance of
24 CD63+/CD81+ sEVs as well as CD63+/CD81+/CD9+ in both fractions (Fig S3A). In contrast, the GuHCl
25 fraction was particularly enriched with CD63+ and CD63+/CD81+ sEVs with very low abundance of
26 CD9+ EVs (Fig S3A). The abundance of CD63+/CD81+ sEVs was confirmed independently by a CD63+
27 bead capture assay in the media and loosely bound fractions (Fig S3B).

28 We previously found that the serum protein prothrombin binds to the sEV surface both in the media
29 and MVB lumen showing it is recycled in sEVs and catalyses thrombogenesis being on the sEV
30 surface⁴³. So we investigated whether FN can also be associated with sEV surface where it can be
31 directly involved in sEV-cell cross-talk⁴³. We treated serum-deprived primary human aortic VSMCs
32 with FN-Alexa568 and found that it was endocytosed and subsequently delivered to early and late
33 endosomes together with fetuin A, another abundant serum protein that is a recycled sEV cargo and
34 elevated in plaques (Figs S3C and S3D). CD63 visualisation with a different fluorophore (Alexa488)
35 confirmed FN colocalization with CD63+ MVBs (Fig S3E). Next, we stained non-serum deprived VSMC
36 cultured in normal growth media (RPMI supplemented with 20% FBS) with an anti-FN antibody and
37 observed colocalization of CD63 and serum-derived FN. Co-localisation was reduced likely due to
38 competitive bulk protein uptake by non-deprived cells (Fig S3F). Notably, when we compared FN
39 distribution in sparsely growing VSMCs versus confluent cells we found that FN intracellular spots, as
40 well as colocalization with CD63, completely disappeared in the confluent state (Fig S3F and S3G).
41 This correlated with nearly complete loss of CD63+/CD81+ sEV secretion by the confluent cells
42 indicating that confluence abrogates intracellular FN trafficking as well as sEV secretion by VSMCs
43 (Fig S3H). Finally, FN could be co-purified with sEVs from VSMC conditioned media (Fig S3I) and
44 detected on the surface of sEVs by flow cytometry confirming its loading and secretion via sEVs (Fig
45 3C).

1 To understand how VSMCs interact with sEVs in the ECM versus in the media we isolated and
2 fluorescently-labelled sEVs and added them either to the ECM or the media and tracked sEV
3 distribution. Super-resolution microscopy (iSIM) revealed that the addition of sEVs to the cell media
4 resulted in fast uptake by VSMCs and delivery to the nuclear periphery (Fig 3D and Fig S3J). This was
5 particularly obvious in 3D projections (Figs S3J). In contrast, purified sEVs added to FN-coated plates
6 resulting in their even distribution across the ECM were not internalised even 24h after cell addition
7 with no perinuclear localisation of ECM-associated sEVs observed (Fig 3E and Fig S3K). No red
8 fluorescence was observed in the absence of added sEVs (Fig 3F).

9 To spatially map the accumulation of sEV markers in the atherosclerotic plaque *in vivo* we collected
10 12 carotid atherosclerotic plaques and adjacent intact vascular segments excised during carotid
11 endarterectomy. Unbiased proteomics analysis confirmed considerable differences between these 2
12 sample groups, revealing 213 plaque-specific and 111 intact arterial-specific proteins (Fig 4A and Fig
13 4B, Tables S1-S5). Differential expression analysis identified 46 proteins significantly overexpressed
14 (fold change ≥ 2 and FDR-adjusted P value ≤ 0.05) in plaques and 13 proteins significantly
15 upregulated in the intact arterial segments (Fig 4C, Table S3). Among the top proteins differentially
16 expressed in plaques were catalytic lipid-associated bioscavenger paraoxonase 1, atherogenic
17 apolipoprotein B-100, HDL-associated apolipoprotein D, iron-associated protein haptoglobin, and
18 inflammation-related matrix metalloproteinase-9 (Table S3). These proteins have previously been
19 implicated in lipid metabolism alterations as well as inflammation in the plaque hence indicating the
20 advanced atherosclerotic plaque signature of the analysed samples. Comparison of the differentially
21 expressed proteins also revealed an accumulation in atherosclerotic regions of fetuin-A (Alpha-2-HS-
22 glycoprotein, P02765, 2.7 fold increase, p=0.003869659), an abundant sEV cargo protein which is
23 recycled by VSMCs²³. Likewise, the level of another sEV cargo, Apolipoprotein B-100 (P04114) was
24 also significantly elevated (2.8 fold increase, p= 0.000124446) in atherosclerotic plaque (Table S2)²³.
25 Notably, a negative regulator of sEV secretion, Coronin 1C (Q9ULV4) was downregulated in the
26 plaque (0.6 fold decrease, p=0.000805372, Table S2) consistent with previous studies that suggested
27 that sEV secretion is upregulated during plaque progression^{40, 44}.

28 To test if FN associates with sEV markers in atherosclerosis, we investigated the spatial association
29 of FN with sEV markers using the sEV-specific marker CD81. Staining of atherosclerotic plaques with
30 haematoxylin and eosin revealed well-defined regions with the neointima as well as tunica media
31 layers formed by phenotypically transitioned or contractile VSMCs, respectively (Fig S4A). Masson's
32 trichrome staining of atherosclerotic plaques showed abundant haemorrhages in the neointima, and
33 sporadic haemorrhages in the tunica media (Fig S4B). Staining of atherosclerotic plaques with orcein
34 indicated weak connective tissue staining in the atheroma with a confluent extracellular lipid core,
35 and strong specific staining at the tunica media containing elastic fibres which correlated well with
36 the intact elastin fibrils in the tunica media (Figs S4C and S4D). Using this clear morphological
37 demarcation, we found that FN accumulated both in the neointima and the tunica media where it
38 was significantly colocalised with the sEV marker, CD81 (Fig. 4D, 4E and 4F). Notably CD81 and FN
39 colocalization was particularly prominent in cell-free, matrix-rich plaque regions (Figs. 4E and 4F).
40 Interestingly, colocalization analysis of CD81 and FN distribution showed that there was a trend of
41 higher colocalization levels of CD81 with FN in the neointima as compared to tunica media which
42 was not significant (Thresholded Mander's split colocalisation coefficient for CD81 colocalization
43 with FN 0.58 ± 0.21 and 0.49 ± 0.14 , respectively, N=13, p=0.052, paired T test). An enhanced
44 expression of CD81 by endothelial cells in early atheroma has been previously reported so to study
45 the contribution of CD81+ sEVs derived from endothelial cells we investigated the localisation of
46 CD31 and CD81⁴⁵. In agreement with a previous study, we found that the majority of CD31
47 colocalises with CD81 (Thresholded Mander's split colocalization coefficient 0.54 ± 0.11 , N=6)

1 indicating that endothelial cells express CD81 (Fig 4G)⁴⁵. However, only a minor fraction of total
2 CD81 colocalised with CD31 (Thresholded Mander's split colocalization coefficient 0.24 ± 0.06 , N=6)
3 confirming that the majority of CD81 in the neointima is originating from the most abundant VSMCs.
4 Finally, western blot analysis confirmed FN accumulation in the plaque region (Figs 4H, 4I and S4E).
5 To understand the origin of plaque FN we performed RT-PCR. FN expression could neither be
6 detected in plaques nor in intact vessels, although it was abundant in the liver (*data not shown*),
7 suggesting that the circulation is a key source of FN in atherosclerotic plaques.

8 **4. sEVs stimulate VSMC directional invasion and induce early peripheral focal adhesion assembly
9 with an enhanced pulling force.**

10 FN as a cargo in sEVs promotes FA formation in tumour cells and increases cell speed^{14,15}. As we
11 found that FN is loaded into VSMC-derived sEVs we hypothesized that ECM-entrapped sEVs can
12 enhance cell migration by increasing cell adhesion and FA formation in the context of a FN-rich ECM.
13 Therefore, we tested the effect of sEV deposition onto the FN matrix on VSMC migration in 2D and
14 3D models. We found that FN coating promoted VSMC velocity and inhibition of bulk sEV secretion
15 with 3-OMS reduced VSMC speed in a 2D single-cell migration model (Figs. 5A, 5B) in agreement
16 with previous studies using tumour cells^{14,15}. However, addition of sEVs to the ECM had no effect on
17 VSMC speed at baseline but rescued cell speed and distance in the presence of the sEV secretion
18 inhibitor, 3-OMS suggesting the EVs are not primarily regulating cell speed (Figs 5A and 5B).

19 To assess the effect of sEVs on cell directionality we exploited a 3D model developed by Sung et al¹⁵
20 and examined VSMC invasion using a μ-Slide Chemotaxis assay where cells were embedded into FN-
21 enriched 3D Matrigel matrices in the absence or presence of exogenously-added sEVs (Fig. 5C). We
22 developed a script to automatically measure cell invasion parameters (track length, cell speed,
23 straightness, accumulated distance, lateral and vertical displacement and parallel forward motion
24 index (FMI)). The addition of sEVs had no effect on cell speed, accumulated distance or straightness
25 (Figs. 5D, 5E, 5F). However, VSMCs invading in the presence of embedded sEVs migrated more
26 aligned to the FBS gradient compared to cells plated in the absence of sEVs. To test whether this was
27 a feature of all EV populations we also performed the experiment in the presence of larger EVs
28 pelleted at the 10,000xg centrifugation step and observed no effect suggesting this mechanism was
29 specific to sEVs (Figs. 5G and 5H). Hence, ECM-associated sEVs have modest influence on VSMC
30 speed but influence VSMC invasion directionality.

31 We wondered whether VSMC migration and invasion were affected by the FN cargo in sEVs that was
32 shown previously to promote tumour cell migration by enhancing FA assembly and cellular adhesion
33 to FN¹⁴. Therefore, we measured VSMC adhesion using an adhesion assay where sEVs were added
34 to FN-coated plates and cells were plated onto these matrices for 1h and firmly attached cells
35 counted. Surprisingly we observed a marked reduction of VSMC adhesion to FN in the presence of
36 sEVs (Fig 6A) suggesting that ECM-associated sEV can impair VSMC adhesion. Mesenchymal cell
37 attachment to the matrix is mediated by transient focal complexes present in the cellular protrusion
38 as well as centripetal FAs that link the cellular cytoskeleton to the matrix and mediate the pulling
39 force to move the cell body^{12,13}. Consistently we observed focal complexes in cellular protrusions as
40 well as more centripetal FAs which were associated with mature actin stress fibres in VSMCs plated
41 onto FN matrix (Fig S5A). Therefore, we used a live cell spreading assay to monitor cellular adhesion
42 over time using ACEA's xCELLigence. As expected, FN alone stimulated VSMC spreading and
43 adhesion (Figs. 6B and 6C). Addition of sEVs did not impact cellular adhesion over the first ~15 min
44 but then the adhesion was stalled in the presence of sEVs (Fig 6B and 6C) suggesting a defect in
45 further cellular spreading. Again, to test whether this was specific for the sEV subset, we also tested

1 the effect of larger EVs pelleted at 10,000x g and found that these EVs had no effect on VSMC
2 adhesion and spreading onto the FN matrix (Fig 6B and 6C). To interrogate the stalling event induced
3 by sEVs in VSMCs we plated cells and counted the number of FAs, average size as well as distance
4 from the cell periphery after 30 mins using TIRF microscopy. Once again plating VSMCs onto FN
5 increased the cell size, number of FAs as well as the number of centripetal FAs as compared to cells
6 spreading over non-coated plastic (Figs 6E-I). Importantly, addition of sEVs to FN significantly
7 reduced the number of FAs and the newly formed FAs were formed in close proximity to the cell
8 periphery (Figs. 6E and 6F). Interestingly, the average FA size was similar between the various
9 conditions (Fig 5I).

10 Cellular traction force is generated by the FA gradient upon FA turnover - formation at the leading
11 edge and disassembly at the tail^{12, 13, 46}. To test if sEVs can influence FA turnover in migrating VSMCs
12 we examined FA turnover in the presence of sEVs. Adhesion sites were visualised by paxillin-RFP
13 reporter expression and the FA turnover index was calculated by counting FA overlap over time
14 using a previously developed algorithm to track individual FAs (Fig S5B)⁴⁷. Interestingly, the FA
15 turnover index remains the same in the presence of sEVs indicating that FA stability was not altered
16 (6J). These data correlate well with no changes observed in FA average size across various conditions
17 (Fig 6I) and indicate that sEVs are not influencing FA assembly or “life-cycle” directly. Rho-dependent
18 activation of actomyosin contractility stabilises FAs by mechanical forces halting fibroblast spreading
19 onto FN^{48, 49}. We hypothesized that sEVs trigger the appearance of premature, peripheral FAs by
20 activating Rho-dependent cellular contractility. To test whether sEVs can modulate mature FA
21 contractility we measured individual traction force which is generated by mature adhesion sites in
22 the absence or presence of sEVs (Fig. S5C). VSMCs transfected with paxillin-RFP were plated on FN
23 and sEV-covered PDMS pillars and pillar displacements were calculated as previously described⁵⁰⁻⁵².
24 Importantly, the traction force was increased in the presence of sEVs (Fig 6K). Altogether these data
25 suggest that ECM-associated sEVs can trigger the formation of FAs with enhanced pulling force at
26 the cell periphery.

27 **5. The sEV cargo Collagen VI regulates focal adhesion formation in VSMCs and cell invasion**

28 To identify the components triggering peripheral FA formation we compared the proteomic
29 composition of sEVs with the larger EV fraction, which had no effect on FA formation. We identified
30 257 proteins in sEVs and 168 proteins in EVs with 142 proteins common between both datasets (Fig
31 7A, Tables S6-S8, Fig S6A). Functional enrichment analysis revealed that the top 5 clusters were
32 related to cell migration - ECM organization, movement of cell or subcellular component, cell
33 adhesion, leukocyte migration and cell-cell adhesion (Fig 7B, Fig S6B, Table S8). The cell adhesion
34 cluster included collagen VI (chains COL6A1, COL6A2 and COL6A3), extracellular matrix glycoproteins
35 (FN and thrombospondin, THBS2, THBS1) as well as EGF-like repeat and discoidin I-like domain-
36 containing protein (EDIL3) and transforming growth factor-beta-induced protein ig-h3 (TGFBI) (Fig
37 7B, Fig S6B, Table S8). Notably, these sEV proteins are predominantly involved in cell-matrix
38 interactions and cellular adhesion. The lectin galactoside-binding soluble 3 binding protein
39 (LGALS3BP) which regulates cell adhesion and motility was also presented exclusively in sEVs (Table
40 S6). These cell adhesion modulating proteins including Collagen VI, TGFBI, EDIL and LGALS3BP were
41 either uniquely or highly enriched in sEVs compared to larger EVs as detected by western blotting
42 (Fig 7C).

43 Collagen VI was the most abundant protein in VSMC-derived sEVs (Fig 7B, Table S7) and was
44 previously implicated in the interaction with the proteoglycan NG2⁵³ and suppression of cell
45 spreading on FN⁵⁴. To confirm the presence of collagen VI in ECM-associated sEVs we analysed sEVs
46 extracted from the 3D matrix using 0.5M NaCl treatment and showed that both collagen VI and FN

1 are present (Fig 7D). Next, we analysed the distribution of collagen VI using dot-blot. Alix staining
2 was bright only upon permeabilization of sEV indicating that it is preferentially a luminal protein (Fig
3 7E). On the contrary, CD63 staining was similar in both conditions showing that it is surface protein
4 (Fig 7E). Interestingly, collagen VI staining revealed that 40% of the protein is located on the outside
5 surface with 60% in the sEV lumen (Fig 7E). To test the role of collagen VI in sEV-induced changes in
6 VSMC spreading we incubated FN-deposited sEVs with an anti-collagen VI antibody to block its
7 interaction with the proteoglycan NG2⁵⁵. Addition of the anti-collagen VI antibody restored VSMC
8 spreading on the FN matrix as compared to non-specific IgG treatment (Fig. 7F). Moreover, sEVs
9 isolated from VSMCs after collagen VI knockdown using siRNA had no effect in the 3D invasion
10 model on cell speed (Fig 7G) or direction (Fig. 7H) but reduced cell alignment to the gradient as
11 compared to VSMCs treated with a scrambled siRNA control (Fig. 7I). Finally, we compared the
12 expression of collagen VI, EDIL3 and TGFBI between the plaque and control aorta tissues (Table S1).
13 Importantly, collagen VI and TGFBI expression were significantly elevated in the plaque (Fig 7J)
14 consistent with increased deposition of sEVs during disease progression. Altogether these data
15 indicate that sEVs can induce early formation of mature peripheral FAs by presenting collagen VI
16 thus acting to modulate cell directionality upon the invasion (Graphical Abstract).

17

1 **Discussion.**

2 VSMC migration and invasion to the site of vascular injury is crucial for vessel repair as well as the
3 pathogenic development of atherosclerotic plaque, however the mechanisms of effective invasion
4 through the complex vascular ECM meshwork have been poorly studied. Here we show that FN, a
5 novel marker of unstable plaques⁶, enables VSMC migration and invasion by stimulating secretion of
6 collagen VI-loaded sEVs which decorate the ECM and stimulate FA maturation. Notably, our data are
7 consistent and extend previous reports showing that EV secretion by tumour cells enhances nascent
8 adhesion formation hence facilitating tumor cell migration and invasion¹⁴⁻¹⁶. In particular, we found
9 that sEVs induce formation of FAs with an enhanced pulling force at the cell periphery thus favouring
10 actomyosin-mediated contractility which is essential for cell body propulsion and locomotion.

11 Mesenchymal cell migration begins with protrusive activity at the leading edge followed by the
12 forward movement of the cell body^{13, 49, 56}. Cell directionality is guided via the integrin $\beta 1$ “probe” on
13 the tip of cellular protrusions, filopodia and lamellipodia⁵⁷. Cellular protrusions are attached to the
14 ECM via focal complexes and extended by the physical force generated by the branched network of
15 actin filaments beneath the plasma membrane⁵⁸. Focal complexes either disassemble or mature into
16 the elongated centripetally located FAs⁴⁸. In turn, these mature FAs anchor the ECM to actin stress
17 fibres and the traction force generated by actomyosin-mediated contractility pulls the FAs rearward
18 and the cell body forward^{12, 13}. Here we report that $\beta 1$ integrin activation triggers sEV release
19 followed by sEV entrapment by the ECM. Curiously we observed CD63+ MVB transport toward the
20 filopodia tips as well as inhibition of sEV-secretion with filopodia formation inhibitors suggesting that
21 sEV secretion can be directly linked to filopodia but further studies are needed to define the
22 contribution of this pathway to the overall sEV secretion by cells. To gain insight into how sEVs can
23 stimulate cell invasiveness we explored VSMC protrusive activity using live cell spreading assays and
24 TIRF imaging. FN stimulated VSMC spreading by increasing the number of FAs, which were formed
25 centripetally from the cell plasma membrane. FN-associated sEV dramatically ceased VSMC
26 spreading by inducing early formation of mature FAs at the cell periphery. Cell spreading and
27 adhesion are orchestrated by the Rho family of small GTPases, Cdc42, Rac1 and Rho with Cdc42 and
28 Rac1 modulating filopodia and lamellipodia and focal complex formation and Rho controlling FA
29 maturation and actomyosin-mediated contractility^{11, 59, 60}. Interestingly, in fibroblasts Rho is
30 specifically degraded in cellular protrusions and cellular spreading on FN is accompanied by transient
31 Rho suppression during the fast cell spreading phase^{49, 61, 62}. This phase is followed by Rho activation
32 leading to formation of actin stress fibres, tension increase on the focal complexes and their
33 maturation into elongated centripetally located FAs^{48, 49, 61, 63}. Excessive Rho activation leads to
34 premature FA assembly and stress fiber formation resulting in reduced cellular protrusions,
35 inhibition of cellular spreading and motility on the FN matrix^{49, 61, 64-66}. Altogether these data indicate
36 that Rho activity, in mesenchymal cells with extensive FA networks such as fibroblasts or VSMCs, can
37 slow down cell migration by immobilising cells¹³. However, we found that sEVs were not influencing
38 mature FA stability. On the contrary, sEV-induced FAs were spatially restricted to the cell periphery
39 near cellular protrusions and were characterised by an enhanced pulling force activity. Interestingly,
40 fibroblast polarization is driven by Smurf1-dependent RhoA ubiquitinylation and localised
41 degradation in cellular protrusions⁶². A recent study indicated that Rho-dependent contractility is
42 essential for cell invasion in a 3D model and it is tempting to speculate that local Rho activity can
43 enable VSMC invasion by stabilizing FAs at the leading edge and stimulating actomyosin-mediated
44 contractility and cell body movement⁶⁷. On the other hand Rho-ROCK activity is critical for the
45 protease-independent rounded motility of tumour cells and cell types with few adhesion contacts
46 (ameboid) when Rho-dependent contractile forces generate hydrostatic pressure forming multiple
47 membrane blebs to invade the ECM^{68, 69}. In fact, we observed that an extensive secretion of sEVs

1 effectively ceased protrusion activity; also VSMCs acquired a rounded morphology when “hovering”
2 over the FN matrix decorated with sEVs (data not shown). Hence, it will be interesting in future
3 studies to investigate whether sEVs can stimulate Rho activity by presenting adhesion modulators—
4 particularly collagen VI—on their surface, thereby guiding cell directionality during invasion.

5 Collagen VI is a nonfibrillar collagen that assembles into beaded microfilaments upon secretion and
6 it plays both structural and signalling roles⁷⁰. Interestingly, type VI collagen deposition by interstitial
7 fibroblasts is increased in the infarcted myocardium and collagen VI knockout in mice improves
8 cardiac function, structure and remodelling after myocardial infarction via unknown pathways^{71, 72}.
9 Immunohistochemical analysis showed that in the healthy vasculature collagen VI is detected in the
10 endothelial basement membrane in the intima and it also forms fibrillar structures between smooth
11 muscle cells in the media. In the fibrous plaque collagen VI is diffusely distributed throughout both
12 the fibrous cap and atheroma⁷³. Curiously, treatment of ApoE-/ mice with antibodies to collagen VI
13 reduced atherosclerosis but its exact role has remained unknown⁷⁴. We and others detected
14 Collagen VI in sEVs but its functional significance remained unknown^{23, 75}. Here we showed that
15 collagen VI is essential for early FA formation at the VSMC periphery as well as VSMC invasion in a
16 3D model. We propose that collagen VI modulates FA formation either by activating cellular
17 signalling or acting as a structural component changing local ECM stiffness¹². Identified collagen VI
18 receptors include $\alpha 3\beta 1$ integrin, the cell surface proteoglycan chondroitin sulfate proteoglycan-4
19 (CSPG4; also known as NG2), and the anthrax toxin receptors 1 and 2⁷⁶⁻⁷⁹. Interestingly, a novel,
20 recently identified Collagen VI signalling receptor (CMG2/ANTXR2) mediates localised Rho activation
21 upon collagen VI binding^{79, 80}. NG2 also activates the Rho/ROCK pathway leading to effective
22 amoeboid invasiveness of tumour cells which is characterised by excessive blebbing and enhanced
23 actomyosin contractility^{68, 81}. Hence, binding of collagen VI to these receptors can potentially locally
24 activate Rho and trigger FA formation and actomyosin contractility thus increasing VSMC motility
25 and directional invasiveness. Of note, it was also reported that NG2 expression is elevated in VSMCs
26 in the atherosclerotic plaque and NG2 knockout prevents plaque formation^{53, 82}. Curiously,
27 endotrophin, a collagen VI $\alpha 3$ chain-derived profibrotic fragment has recently been associated with
28 a higher risk of arterial stiffness and cardiovascular and all-cause death in patients with diabetes
29 type 1 and atherosclerosis, respectively^{83, 84}.

30 In addition to collagen VI the unique adhesion cluster in VSMC-derived sEVs also includes EGF-like
31 repeat and discoidin I-like domain-containing protein (EDIL3), transforming growth factor-beta-
32 induced protein ig-h3 (TGFB1) and the lectin galactoside-binding soluble 3 binding protein
33 (LGALS3BP) and these proteins are also directly implicated in activation of integrin signalling and
34 cellular invasiveness⁸⁵⁻⁸⁷. Although we found that collagen VI plays the key role in sEV-induced early
35 formation of FAs in VSMCs, it is tempting to speculate that the high sEV efficacy in stimulating FA
36 formation is driven by cooperative action of this unique adhesion complex on the sEVs surface and
37 targeting this novel sEV-dependent mechanism of VSMC invasion may open-up new therapeutic
38 opportunities to modulate atherosclerotic plaque development or even to prevent undesired VSMC
39 motility in restenosis.

40 We also identified a positive feedback loop and showed that FN stimulates sEV secretion by VSMCs.
41 sEV secretion is a tightly regulated process which is governed by activation of signalling pathways
42 including activation of G-protein coupled receptors³⁹ and alterations in cytosolic calcium⁸⁸, small
43 GTPases Rab7, Rab27a, Rab27b and Rab35^{89, 90}, vesicular trafficking scaffold proteins including
44 syntenin⁹¹, sortillin⁹² and CD63⁹³ or accumulation of ceramide²⁶. We found that the fibrillar ECM
45 proteins, FN and collagen I induce sEV secretion by activating the $\beta 1$ integrin/FAK/Src and Arp2/3-
46 dependent pathways. Our *in vivo* FN staining data are in good agreement with previous studies

1 showing accumulation of FN in late-stage plaques^{6, 7}. Moreover, we observed close co-distribution of
2 FN and CD81 in the plaque suggesting that accumulating FN matrices can stimulate sEV secretion *in*
3 *vivo*. Notably, expression of the major FN receptor, $\alpha 5\beta 1$ integrin is re-activated upon VSMC de-
4 differentiation following vascular injury⁹⁴. It is thought the $\alpha 5\beta 1$ integrin mediates FN matrix
5 assembly, whilst $\beta 3$ integrins are important for cell-matrix interactions^{94, 95}. Our data sheds new light
6 on the functional role of $\alpha 5\beta 1$ as an ECM sensor inducing production of collagen VI-loaded sEVs
7 which in turn enhance cell invasion in the complex ECM meshwork. Although our small inhibitors
8 and integrin modulating antibody data clearly indicate that $\beta 1$ activation triggers sEV secretion via
9 activation of actin assembly we cannot fully rule out that FN may also be modulating growth factor
10 activity which in turn contributes to sEV secretion by VSMCs²³. Excessive collagen and elastin matrix
11 breakdown in atheroma has been tightly linked to acute coronary events hence it will be interesting
12 to study the possible link between sEV secretion and plaque stability as sEV-dependent invasion is
13 also likely to influence the necessary ECM degradation induced by invading cells⁹⁶.

14 In summary, cooperative activation of integrin signalling and F-actin cytoskeleton pathways results in
15 the secretion of sEVs which associate with the ECM and play a signalling role by controlling FA
16 formation and cell-ECM crosstalk. Further studies are needed to test these mechanisms across
17 various cell types and ECM matrices.

18

19

1 **Materials and Methods**

2 **Materials**

3 Proteins were fibronectin (Cell Guidance Systems, AP-23), collagen I (Gibco, #A1048301), laminin
4 (Roche, 11243217001), Matrigel (Corning, #356237), Phalloidin-rhodamin (ThermoFisherScientific,
5 R415). Peptides were Gly-Arg-Gly-Asp-Ser-Pro (GRGDSP, Merck, SCP0157) and scramble control Gly-
6 Arg-Ala-Asp-Ser-Pro (GRADSP, Merck, SCP0156). All chemical inhibitors were diluted in DMSO and
7 were: 3-O-Methyl-Sphingomyelin (SMPD3 inhibitor, Enzo Life technologies, BML-SL225-0005),
8 FAM14 inhibitor (FAK inhibitor, Abcam, ab146739), PP2 (Src inhibitor, Life technologies, PHZ1223),
9 CK666 (Arp2/3 inhibitor, Abcam ab141231), SMIFH2 (Formin inhibitor, Sigma, S4826). Control siRNA
10 pool (ON-TARGETplus siRNA, Dharmacon, D-001810-10-05), collagen VI siRNA ON-TARGETplus siRNA
11 (COL6A3, Human), SMARTPool, Horizon, L-003646-00-0005). Antibodies were CD9 (SA35-08 clone,
12 NBP2-67310, Novus Biologicals), CD63 (BD Pharmingen, 556019), CD81 (BD Pharmingen™, 555676,
13 B-11, SantaCruz, sc-166029 and M38 clone, NBP1-44861, Novus Biologicals), Syntenin-1 (Abcam,
14 ab133267), Syndecan-4 (Abcam, ab24511), α -Actinin-4 (Abcam, ab108198), fibronectin (Abcam,
15 ab2413, ab6328 [IST-9] (3D matrix staining) and F14 clone, ab45688 (clinical samples analysis)), β 1
16 activating (12G10) antibody was previously described⁹⁷, 4B4 integrin inhibiting antibody (Beckman
17 Coulter, 41116015), vinculin (Sigma, V9264), α 5 integrin (P1D6, Abcam, ab78614), Myo10 (Sigma,
18 HPA024223), gelatin-3BP/MAC-2BP (R&D systems, AF2226), EDIL3 antibody (R&D systems,
19 MAB6046), TGFBI (Sigma, SAB2501486), IgG mouse (Sigma PP54), Anti-collagen Type VI antibody,
20 clone 3C4 (Sigma, MAB1944) (functional blocking), Anti-collagen Type VI antibody (Abcam, AB6588)
21 (western blot) Anti-collagen Type VI antibody (Abcam, AB182744) (dot blot) p34-Arc/ARPC2
22 antibody (Millipore, #07-227), Cortactin, LGALS3BP (R&D, AF2226), GAPDH (ab139416, Abcam), Alix
23 (Clone 3A9, ThermoFisher Scientific, MA1-83977) Donkey Anti-mouse Secondary IRDye@680 LT (Li-
24 COR, 926-68022) and Donkey Anti-Rabbit Secondary IRDye@800 CW (Li-COR, 926-32213) DNA
25 plasmids were: CD63-GFP was kindly provided by Dr Aviva Tolkovsky⁹⁸, CD63-pHluorin was
26 previously described³⁹, CD63-RFP was previously published⁹⁹, Paxillin-RFP was previously
27 described⁹⁷, ARPC2-GFP DNA vector was kind gift from Professor Michael Way laboratory³⁴, F-
28 tractin-RFP was kindly provided by Dr Thomas S. Randall (King's College London, UK), Myo10-GFP
29 (Addgene Plasmid#135403) was previously described¹⁰⁰.

30 **Cell culture**

31 Human VSMCs were isolated as previously described¹⁰¹ and were cultured in Dulbecco's modified
32 Eagle medium (Sigma) supplemented with 20% fetal calf serum, 100 U/ml penicillin, 100 μ g/ml
33 streptomycin and 2 mmol/L L-glutamine (Gibco) and used between passages 4 and 12.

34 **VSMC adhesion**

35 24 well plate (Corning Costar) was incubated with 5 μ g/ml fibronectin in PBS overnight at +4°C. Next,
36 sEVs (10 μ g/ml) diluted in PBS were added to the wells and incubated overnight at +4°C. Wells were
37 washed with PBS, blocked with PBS-1% BSA for 30min at 37°C and washed 3 times with PBS again.
38 VSMCs were incubated in serum free media, M199 supplemented with 0.5% BSA, 100 U/ml penicillin
39 and 100 μ g/ml streptomycin overnight and removed by brief trypsin treatment. Next, 20,000 cells
40 were added to each well and incubated for 30min at +37°C. Unattached cells were washed away
41 with PBS and attached cells were fixed with 3.7% PFA for 15 min at 37°C. Cells were washed with
42 H₂O 3 times and stained with 0.1% crystal violet for 30min at 10% CH₃COOH for 5min at room
43 temperature. Samples were transferred to 96 well plate and absorbance was measured at 570nm
44 using the spectrophotometer (Tecan GENios Pro).

1 ***iCELLigence adhesion protocol***

2 E-Plate L8 (Acea) was coated with FN (5 μ g/mL) in PBS at 4°C overnight. Next, E-Plate L8 was gently
3 washed once with cold PBS followed by the incubation with EV or sEV (10 μ g/ml) at 4°C overnight.
4 The following day, E-Plate L8 was incubated with 0.1% BSA in PBS for 30min at 37°C to block non-
5 specific binding sites and washed with PBS before adding 250 μ L of M199 media supplemented with
6 20% exosome-free FBS. VSMCs were serum-deprived by incubation in M199 media supplemented
7 with 0.5% BSA overnight, were passaged with trypsin and resuspended in media M199
8 supplemented with 20% exosome-free FBS to a final concentration 80,000 cells/mL. Cell aliquot
9 (250 μ L) was added to E8-plate L8 which was then transferred to iCELLigence device for the adhesion
10 assay. Cell adhesion was measured at 37°C with time intervals 20sec for 1h.

11 ***Focal adhesion turnover assay***

12 iBIDI 35mm dishes were incubated with FN (5 μ g/ml) in PBS overnight at +4°C and treated with
13 exosomes (10 μ g/ml) diluted in PBS overnight at +4°C. 500,000 cells were transfected with Paxillin-
14 RFP/Myo10-GFP by using electroporation (see below) and plated on iBIDI 35mm dishes coated with
15 FN and sEVs in DMEM supplemented with 20% exosome-free FBS, 100 U/ml penicillin, and 100
16 μ g/ml streptomycin. Next, cells were transferred to DMEM supplemented with 20% exosome-free
17 FBS, 10mM HEPES, 100 U/ml penicillin, and 100 μ g/ml streptomycin and images were acquired
18 (Nikon Spinning Disk) every 1min for 30min at 37°C. FA images were extracted from timelapses and
19 FA turnover was quantified using Mathematica by producing the adhesion map as previously
20 described⁴⁷.

21 ***Confocal spinning disk microscopy and live cell imaging***

22 VSMC were transfected using electroporation (see below) and plated onto FN-coated 35mm iBIDI
23 glass bottom dish and incubated for 48h. Then cells were transferred to DMEM supplemented with
24 20% exosome-free FBS, 10mM HEPES, 100 U/ml penicillin, and 100 μ g/ml streptomycin and images
25 were acquired every 1min for 20min at 37°C using a Nikon Ti-E (inverted) microscope equipped with
26 a Yokogawa spinning disk and a Neo 5.5 sCMOS camera (Andor) and 60x or 100x/1.40 NA Plan Apo λ
27 oil objectives (Nikon) were used. Images were acquired using NIS Elements AR 4.2 software. Cells
28 were maintained at 37°C, 5% CO₂ throughout the experiment via a CO₂ chamber and a temperature-
29 regulated Perspex box which housed the microscope stage and turret.

30 ***iSIM***

31 Slides was imaged and super-resolved images collected using a Visitech-iSIM module coupled to a
32 Nikon Ti-E microscope using a Nikon 100x 1.49NA TIRF oil immersion lens. Blue fluorescence was
33 excited with a 405nm laser and emission filtered through a 460/50 filter. Green fluorescence was
34 excited with a 488nm laser and emission filtered through a 525/50 filter. Red Fluorescence was
35 excited with a 561nm laser and emission filtered through a 630/30 filter. Far Red fluorescence was
36 excited with a 640nm laser and emission filtered through a 710/60 filter. Images were collected at
37 focal planes spaced apart by 0.08 μ m. Data was deconvolved using a Richardson-Lucy algorithm
38 utilizing 20 iterations using the Nikon deconvolution software module (Nikon Elements). 65 stack
39 images were taken with Z step 0.08 μ m. ImageJ (153t) or NIS Elements (5.21.00, built1483, 64bit)
40 software were used for image analysis and assembly.

41 ***Cell electroporation***

42 iBidi dishes were coated with FN (5 μ g/ml) in PBS for 1 hour at 37°C or overnight at 4°C. VSMCs were
43 grown to 70% confluence, washed twice with EBSS and detached by trypsin treatment for 5min at

1 +37°C. Cells (500,000) were mixed with plasmids (2.5µg each) in electroporation buffer (100µl,
2 Lonza) and transfected using either Nucleofector II (program U25) or Nucleofector III (program CM-
3 137).

4 ***Isolation of apoptotic bodies, extracellular vesicles and small extracellular vesicles***

5 Flasks (T150) were incubated with PBS or FN (5µg/ml) in PBS overnight at +4°C and VSMCs ($\approx 10^6$
6 cells) were plated and incubated for 16h at +37°C. Next, cells were washed with EBSS 3 times and
7 incubated with DMEM supplemented with 0,1% BSA, 100 U/ml penicillin, and 100 µg/ml
8 streptomycin. Conditioned media was collected and centrifuged at 2,500 rpm (Thermo Scientific
9 Heraeus Multifuge 3SR+ centrifuge, rotor Sorvall 75006445) for 5min to remove apoptotic bodies
10 (AB, 1.2K pellet). Supernatant was transferred to centrifugation tube (Nalgene™ Oak Ridge High-
11 Speed Polycarbonate Centrifuge Tubes, Thermo Fisher Scientific, 3138-0050) and centrifuged 10,000
12 xg for 30min. 10K pellet (EVs) was collected, washed in PBS once and kept at -80°C until further
13 analysis. 10K supernatant was transferred to ultracentrifugation tubes (Polycarbonate tubes for
14 ultracentrifugation, BeckmanCoulter, 355647) and centrifuged at 35,000 rpm (100,000xg) for 40min
15 at 4°C (Fixed-angle rotor, Beckman Coulter Optima Max Unltracentrifuge). 100K pellet (sEVs) was
16 washed with PBS twice and re-suspended in PBS. EV and sEV pellets were kept at -80°C for the
17 proteomic analysis and freshly isolated sEVs were used for all other assays.

18 ***EV and sEV proteomic analysis***

19 EV and sEV samples were submitted to the CEMS Proteomics Facility in the James Black Centre,
20 King's College London for mass spectrometric analysis. The data were processed by Proteome
21 Discover software for protein identification and quantification. Scaffold 5 proteome software was
22 utilized to visualize differential protein expression. Individual proteins intensities were acquired and
23 transformed to log2 scale before Hierarchical clustering analysis based on Euclidean distance and k-
24 means processing. Differential genes defined by multiple groups comparation were applied to
25 perform the gene ontology functional assay through using the DAVID Gene Ontology website
26 (<https://david.ncifcrf.gov/>). Selected genes which showed abundant in each condition were applied
27 to generate Venn diagram through Interacti website (<http://www.interactivenn.net/>).

28 ***Cell lysis***

29 Cells were washed with PBS and removed by cell-scraper in 1ml of PBS. The cells were pelleted by
30 centrifugation at 1000xg for 5min and cell pellets were kept at -80°C until further analysis. To
31 prepare cell lysates, pellets were incubated with lysis buffer (0.1M TrisHCl(pH8.1), 150 mM NaCl, 1%
32 Triton X-100 and protease inhibitors cocktail (Sigma, 1:100)) for 15min on ice. Cell lysates were
33 subjected to ultrasound (Branson Sonifier 150), centrifuged at 16,363xg for 15 minutes (Eppendorf)
34 at 4°C and supernatants were collected and analysed by western blotting.

35 ***CD63-bead capturing assay***

36 CD63-bead capturing assay was conducted as previously described²³ with some modifications. In
37 brief, CD63 antibody (35µg) was immobilised on 1×10^8 4µm aldehyde-sulfate beads (Invitrogen) in
38 30mM MES buffer (pH 6.0) overnight at room temperature and spun down by centrifugation
39 (3,000xg, 5min). Next, beads were washed 3 times with PBS containing 4%BSA and kept in PBS
40 containing 0,1% Glycine and 0,1% NaN₃ at +4°C. VSMCs were plated onto 24 well plate (10,000 cells
41 per well) and incubated in the complete media overnight. Next, cells were washed 3 times with EBSS
42 and incubated in M199 supplemented with 2.5% exosome-free FBS in the presence of absence of
43 inhibitors for 2h. Then, conditioned media was replaced once to the fresh aliquot of 2.5% exosome-

1 free FBS in the presence or absence of inhibitors and cells were incubated for 18-24h. VSMC
2 conditioned media was collected and centrifuged and centrifuged at 2,500xg for 5 min. VSMCs were
3 detached from the plate by trypsin treatment and viable cells were quantified using NC3000
4 (ChemoMetec A/S). The conditioned media supernatants were mixed with 1 μ L of anti-CD63-coated
5 beads and incubated on a shaker overnight at +4°C. Beads were washed with PBS-2%BSA and
6 incubated with anti-CD81-PE antibody (1:50 in PBS containing 2% BSA) for 1h at room temperature.
7 Next, beads were washed with PBS-2%BSA and PBS and analysed by flow cytometry (BD Accuri™ C6).
8 sEV secretion (fold change) was calculated as ratio of Arbitrary Units (fluorescence units x
9 percentage of positive beads and normalized to the number of viable VSMCs) in the treatment and
10 control conditions.

11 ***Exosome labelling with Alexa Fluor® 568 C5 Maleimide***

12 Exosomes (10 μ g/ml) were incubated with 200 μ g/mL Alexa Fluor® 568 C5 Maleimide
13 (ThermoFisherScientific, #A20341) in PBS for 1h at room temperature. An excessive dye was
14 removed by using Exosome Spin Columns (MW 3000, ThermoFisherScientific, #4484449) according
15 to the manufacturer protocol.

16 ***Fetuin-A and Fibronectin labelling and uptake studies.***

17 Bovine fetuin-A (Sigma) and Fibronectin were labelled using an Alexa488 (A10235) and Alex568
18 (A10238) labelling kits in accordance with the manufacturer's protocol (Invitrogen). VSMCs were
19 serum-starved for 16h and then incubated with Alexa488-labeled fetuin-A (10 μ g/mL) and Alexa555-
20 labeled fibronectin (10 μ g/mL) from 30 to 180 minutes at 37°C.

21 ***VSMC and beads-coupled sEVs flow cytometry.***

22 VSMC were removed from the plate by brief trypsin treatment, washed with M199 media
23 supplemented with 20% FBS and resuspended in HBSS supplemented with 5%FBS. Cells were kept
24 on ice throughout the protocol. Next, cells (200,000) were incubated with primary antibody for
25 30min on ice, washed with HBSS-5%FBS and incubated with secondary fluorescently-labelled
26 antibody 30min on ice. Then cells were washed twice with HBSS-5%FBS and once with PBS and
27 analysed by flow cytometry (BD FACScalibur, BD Bioscience).

28 Flow cytometry analysis of beads-coupled sEVs was conducted as described before¹⁰². In brief,
29 exosomes (10 μ g) isolated by differential centrifugation were coupled to 4 μ m surfactant-free
30 aldehyde/sulfate latex beads (Invitrogen) and were incubated with primary antibody and
31 fluorescently labeled secondary antibody and analysed by flow cytometry on BD FACScalibur (BD
32 Bioscience). Data were analysed using the Cell Quest Software (BD). Cells and beads stained with
33 isotype-control antibodies were used as a negative control in all experiments.

34 ***Nanoparticle Tracking Analysis***

35 Exosomes were diluted 1:150 and analysed using LM-10 using the light scattering mode of the
36 NanoSight LM10 with sCMOS camera (NanoSight Ltd, Amesbury, United Kingdom). 5 frames (30 s
37 each) were captured for each sample with camera level 10 and background detection level 11.
38 Captured video was analysed using NTA software (NTA 3.2 Dev Build 3.2.16).

39 ***Western blotting and dot blotting***

40 For western blotting, cell lysates or apoptotic bodies, microvesicles and exosomes in Laemmlie
41 loading buffer were separated by 10% SDS-PAGE. Next, separated proteins were transferred to ECL
42 immobilon-P membranes (Millipore) using semi-dry transfer (BioRad). Membranes were incubated

1 in the blocking buffer (TBST supplemented with 5% milk and 0.05% tween-20) for 1h at room
2 temperature, then incubated with primary antibody overnight at +4°C. Next, membranes were
3 washed with blocking buffer and incubated with secondary HRP-conjugated antibody and washed
4 again in PBS supplemented with 0.05% tween-20 and PBS. Protein bands were detected using ECL
5 plus (Pierce ECL Western Blotting Substrate, #32109). Alternately, membranes were incubated with
6 the secondary fluorescent antibody (Alexa fluor antibody) and washed again with TBST or PBST.
7 Blots were detected using Odyssey Licor.

8 Dot blot was conducted as previously described¹⁰³. In brief, an aliquot of isolated sEVs (0.5ug) was
9 absorbed onto nitrocellulose membrane (Odyssey® P/N 926-31090) for 30min at room temperature
10 and air dried. Next, membranes were blocked with PBS-3% BSA in PBS and incubated with primary
11 antibodies (anti-CD63 1:500, anti-COLVI 1:200, anti-Alix, 1:500) in the absence or presence 0.2%
12 (v/v) Tween-20 for 16h at the cold room (+4C) room temperature. Membranes were washed 3 times
13 in PBS-3% BSA, and were incubated with Donkey Anti-Rabbit Secondary IRDye@800 CW (Li-COR,
14 926-32213) and Donkey Anti-Mouse Secondary IRDye@680 LT (Li-COR, 926-68022) (1:10,000),
15 washed with PBS-0.2% tween20 and PBS and visualized and quantified using Odyssey® CLx Infrared
16 Imaging System.

17 ***Generation of 3D Extracellular Matrix***

18 Generation of 3D matrices were conducted as previously described²⁴ with some modifications. In
19 brief, plates or glass coverslides were covered with 0.2% gelatin in PBS for 1h at 37°C. Wells were
20 washed with PBS and fixed with 1% glutaraldehyde in PBS for 30min at room temperature. Plates
21 were washed with PBS and incubated with 1M ethanolamine for 30min at room temperature, then
22 washed with PBS again. VSMCs (5×10^5 per well) were plated and cultured for 24h. Then the medium
23 was replaced with medium containing 50 μ g/ml of ascorbic acid and cells were incubated for 9days.
24 The medium was replaced every 48h. To extract matrix, cells were rinsed with PBS and incubated
25 with pre-warmed extraction buffer (20mM NH₄OH containing 0.5%Triton X-100) for 3min until intact
26 cells are not seen. Next, equal volume of PBS was added to extraction buffer and plates were
27 incubated for 24h at +4°C. Plates were washed with PBS twice and kept with PBS containing 100
28 U/ml penicillin and 100 μ g/ml streptomycin up to 2 weeks at +4 °C.

29 ***sEVs isolation from 3D Extracellular Matrix***

30 VSMCs were cultured on dishes pre-coated with 0.1% gelatin as described above, with minor
31 modifications. Briefly, cells were maintained in DMEM supplemented with EV-free fetal bovine
32 serum, 1% penicillin-streptomycin, and 50 μ g/ml ascorbic acid. Cultures were maintained for 10
33 days, with media changes and collections performed every 2–3 days. At the end of the culture
34 period, the medium was gently removed and collected as the “Media” fraction. Conditioned media
35 was clarified by centrifugation at 2,500 \times g for 15 minutes to remove cellular debris; the resulting
36 supernatant was retained for ExoView analysis and small EV (sEV) isolation. The cell monolayer was
37 then rinsed with phosphate-buffered saline (PBS) and incubated with extraction buffer (0.5 M NaCl,
38 20 mM Tris, pH 7.5) for 4 hours at room temperature as previously described⁴². This NaCl-extracted
39 ECM fraction, termed the “loosely-bound sEV fraction”, was collected and centrifuged at 2,500 \times g
40 for 15 minutes. The supernatant was retained for ExoView analysis and sEV isolation. Following NaCl
41 extraction, cells were treated with 0.1% sodium dodecyl sulfate and 25 mM
42 ethylenediaminetetraacetic acid (EDTA), incubating at 37°C for 10 minutes to lyse any remaining
43 cellular material. To extract the remaining ECM-associated fraction, the matrix was incubated with 4
44 M guanidine hydrochloride (GuHCl) in 50 mM sodium acetate buffer (pH 5.8) for 48 hours at room
45 temperature. The GuHCl fraction, referred to as “strongly-bound sEV fraction” was collected and

1 centrifuged at 2,500 × g for 15 minutes at 4°C; the supernatant was retained for ExoView analysis.
2 sEVs from all fractions were isolated by ultracentrifugation as described above.

3 ***ExoView analysis of ECM-derived sEV fractions***

4 ECM-derived EV fractions (media, loosely bound and strongly trapped sEVs) were prepared as
5 detailed above. For ExoView analysis, each fraction was diluted 1:2 in the manufacturer-supplied
6 incubation solution. Leprechaun Exosome Human Tetraspanin chips (Unchained Labs, REF 251-1044)
7 were used according to the manufacturer's protocol.

8 Briefly, 35–50 μ L of diluted sample (1:2-1:10) was applied to each chip well. Chips were incubated
9 overnight at room temperature in a sealed humidity chamber to allow EV capture onto surface-
10 immobilized antibodies. The following day, chips were washed per the supplied protocol to remove
11 unbound material.

12 Secondary immunostaining was performed using fluorescently labeled antibodies provided in the
13 Leprechaun Exosome Human Tetraspanin Kit (CD9, CD63, and CD81, Unchained Labs, LOT
14 UL038460001F). After antibody incubation, chips were washed thoroughly as recommended and air-
15 dried briefly.

16 Chips were scanned on an ExoView R200 platform (Unchained Labs). Imaging and data analysis were
17 performed using ExoView Analyzer software, with spot intensity and particle counts determined for
18 each tetraspanin (CD9, CD63, CD81) according to the manufacturer's guidelines. Data were exported
19 for downstream quantitative and statistical analysis.

20 ***Immunocytochemistry***

21 VSMCs (10,000 cells per well) were plated onto the coverslips and incubated for 48h. Next, cells
22 were treated with inhibitors in M199 supplemented with 2.5% exosome-free FBS and fixed using
23 3.7% paraformaldehyde for 15 minutes at +37°C. Cells were then washed with PBS, permeabilised
24 with PBS-0,1% triton X-100 for 5 min at room temperature and washed with PBS again. Cells were
25 blocked with PBS-3% BSA for 1 hour at room temperature and incubated with primary antibodies
26 overnight at +4°C. Following washing 3 times with PBS-3% BSA cells were incubated with secondary
27 fluorescently-labelled antibodies in the dark for 1 hour at room temperature, stained with DAPI for
28 5min and mounted onto 75-Superdex slides using gelvatol mounting media and analysed by spinning
29 disk confocal microscopy as above (Nikon). Primary antibodies were used in the following dilutions:
30 CD63 1:500, Cortactin 1:500, Arp2C 1:500, Myo10 1:250, Vinculin 1:500, fibronectin 1:500, CD81
31 1:500, Rhodamine phalloidin 1:200 and secondary fluorescently labelled antibodies 1:200.

32 ***Focal adhesion turnover/Individual traction force***

33 PDMS pillar (500 nm diameter, 1.3 μ m height, 1 μ m centre-to-centre) substrates were prepared as
34 described previously¹⁰⁴. Briefly, CdEq3: $T_{tilt}(\nu) = a \frac{(1+\nu)}{2\pi} \left\{ 2(1-\nu) + \left(1 - \frac{1}{4(1-\nu)} \right) \right\}$ SeS/ZnS alloyed
35 quantum dots (490nm, Sigma) were spun on the master 30s at 10,000rpm with a 150i spin processor
36 (SPS), before the addition of PDMS. PDMS (Sylgard 184, Dow Corning) was mixed thoroughly with its
37 curing agent (10:1), degassed, poured over the silicon master, placed upside-down on a plasma-
38 treated coverslip-dish (Mattek), or coverslip 4-well dishes (Ibidi) and cured at 80C for 2h. The mold
39 was then removed and the pillars were incubated with fibronectin for 1h at 37C, after which pillars
40 were incubated with sEVs (10 μ g/ml in PBS) at 4°C overnight.

41 VSMC previously transfected with Paxillin-RFP by using electroporation as above were plated on the
42 Pillars and imaged on a Nikon Eclipse Ti-E epifluorescent microscope with a 100x 1.4NA objective,
43 Nikon DS-Qi2 Camera and a Solent Scientific chamber with temperature and CO₂ control. For

1 calculation of pillar displacements, a perfect grid was assumed and deviations from the grid were
2 calculated using reference pillars outside the cell. The traction stress was calculated for a 10 μm
3 wide region at the cell edge that was enriched in paxillin staining, taking into account all pillar
4 displacements above a \sim 20 nm noise level, which was calculated from pillars outside the cells.
5

6 The Stiffness of the pillars was calculated as described by Ghibaudo et al⁵² but taking into account
7 substrate warping as described by Schoen et al (Eq1-5)⁵¹:

8 Eq1: $k_{bend} = \frac{3}{64} \pi E \frac{D^4}{H^3}$;

9
10 Eq2: $corr = \frac{\frac{16}{3} \left(\frac{L}{D}\right)^3}{\left(\frac{16}{3} \left(\frac{L}{D}\right)^3 + \frac{7+6\nu L}{3} D + 8T_{tilt}(\nu) \left(\frac{L}{D}\right)^2\right)}$;

11
12 Eq3: $T_{tilt}(\nu) = a \frac{(1+\nu)}{2\pi} \left\{ 2(1-\nu) + \left(1 - \frac{1}{4(1-\nu)}\right) \right\}$

13 Eq4: $k = k_{bend} * corr$;

14 Eq5: $E_{Eff} = \frac{9k}{4\pi a}$;

17 **Protein concentration**

18 Protein concentration was determined by DC protein assay (BioRad).

19 **Focal adhesion TIRF Imaging**

20 μ -Slides (iBidi) were coated with FN (5 $\mu\text{g}/\text{mL}$) in PBS at 4°C overnight. Next, μ -Slides were gently
21 washed once with cold PBS following incubation with EV or sEV at 4°C overnight. The following day
22 μ -Slides were incubated with 0.1% BSA in PBS for 30 minutes at 37°C to block non-specific binding
23 sites and washed with PBS three times and 250 μL of M199 media supplemented with 20% sEV-free
24 FBS was added to each well. VSMCs were incubated in M199 media supplemented with 0.5% BSA
25 overnight, detached with trypsin and resuspended to 80,000 cells/mL in M199 supplemented with
26 20% FBS. Cells (250 μL) were added to μ -Slides and were incubated for 30min at 37°C. VSMC were
27 fixed with 4% PFA for 10 minutes at 37°C, washed with PBS three times and were permeabilised with
28 PBS supplemented with 0.2% Triton X-100 for 10 minutes at 37°C. Next, VSMC were washed three
29 times with PBS for 5 minutes and were incubated with 3% BSA in PBS for 1h at room temperature.
30 VSMC were incubated with anti-vinculin antibody (1:400) in blocking buffer at 4°C overnight. Next,
31 VSMC were washed with PBS for 5min and incubated with secondary antibody (1:500,
32 AlexaFluor488) diluted in blocking buffer for 1h at room temperature. Cells were incubated with
33 CellMaskRed (ThermoFisherScientific) and DAPI (0.1 mg/mL) for 5min, washed and analysed by TIRF
34 microscopy.

35 TIRF Microscopic images were collected on a Nikon Ti2 upright microscope with a TIRF illuminator
36 (Nikon) attached using a 100x oil immersion (1.49 NA) objective lens. In each fluorescent channel the
37 sample was excited with a laser beam at an angle indicated as follows (488nm at 62.3°, 561nm at
38 62.5° and 640nm at 65.5°). All emission light was filtered through a quad channel filter set (Chroma
39 89000) in the upper filter turret and a secondary bandpass emission filter in the lower turret position
40 was used as follows for each channel (488nm excited: filter BP 525/50 - Chroma; 561nm excited:
41 filter BP 595/50 - Chroma; 640nm excited: filter BP 700/75 - Chroma). Light was then passed to a

1 Hamamatsu Orca-Flash 4v3.0 sCMOS camera and exposures for channels was set as follows (488nm:
2 100ms, 561nm: 100ms, 640nm:50ms) with 16bit channel images collected.

3 Acquisition was all controlled through NIS-Elements software (Nikon). Analysis of TIRF images was
4 completed using NIS-Elements General Analysis Module. A general description of the process
5 follows: Cell Area measurements were determined by use of an intensity threshold on the HCS
6 CellMask Deep Red channel at an intensity of 100 AU (grey levels or arbitrary units) above the
7 background to mask the cell. The Cell area, whole cell Vinculin and Far-Red intensity measurements
8 calculated from this binary region. In addition, an inversion of the cell mask binary was generated to
9 have a means to measure distance to edge of the cell.

10 Vinculin derived Foci were masked using an intensity-based threshold (Above 10000 AU) and a size
11 minimum for objects was set to 0.5 μm^2 to eliminate smaller non foci objects from the binary mask.
12 The foci mask was then limited to the cell mask regions to allow interpretation of the foci in the cell
13 area. Minimum Distance to the outside of the cell for each foci was calculated by measurement of
14 the nearest distance to the inverted non-cell mask. The average distance was then recorded for each
15 image. For each foci intensity measurements were taken for the Vinculin and FarRed channel and
16 the Mean intensity of the foci were recorded.

17 **2D VSMC migration time lapse assay**

18 24 well plates were incubated with FN (5 $\mu\text{g}/\text{ml}$) in PBS overnight at +4°C and treated with sEVs
19 (10 $\mu\text{g}/\text{ml}$) diluted in PBS overnight at +4°C. VSMC (8,000 cells per well) were plated on the plate in
20 M199 supplemented with 20% exosome-free FBS and incubated for 16h. Cells were washed twice
21 with DMEM supplemented with 2.5% exosome-free FBS and incubated in this media for 2hrs +/- 3'-
22 OMS. Media was replaced for a fresh aliquot and cells were imaged using Opera Phenix High Content
23 Screening System (PerkinElmer) every 6min20sec for 8h in a transmitted light channel.
24 Quantification of cellular velocity and directionality was performed in Harmony 4.9 (Perkin Elmer)
25 and the following filters were applied to the raw data: "Number of Timepoints" >= 5, "First
26 Timepoint" < 5.

27 **3D VSMC Invasion time lapse assay**

28 *Acquisition.* Migration assay were completed using IBidi Chemotaxis μ -slides (Ibidi μ -slides #80326).
29 VSMC were deprived overnight in M199 supplemented with 0.5% BSA, counted and mixed with
30 Matrigel supplemented with/without sEV (5 μg total in 100 μl volume) to a final cell concentration of
31 ca. 3×10^6 cells/ml and stained with Draq5 according to the manufacturer protocol. Slides were left
32 for 30min at 37°C for gelation and chemoattractant-free medium (65 μl of M199 supplemented with
33 0.5% BSA) was filled through Filling Port E. Next, the empty reservoir was filled by injecting
34 chemoattractant medium (65 μl of M199 supplemented with 20% FBS exosome-free through Filling
35 Port C. 3 slides were loaded and cells were imaged with the Opera Phenix (Perkin Elmer) high
36 content imaging platform (10x Objective NA 0.3). Images were collected for digital phase contrast
37 and a fluorescence channel for Draq5. Fluorescence was obtained by exciting with a 640nm laser and
38 emission light was filtered with a 700/75 bandpass filter to a sCMOS camera. Images were recorded
39 every 10min for 12h in several locations for each slide.

40 *Migration tracking and analysis of tracking.* Analysis of cell motion was completed on Draq5 images
41 using Harmony Software (Perkin Elmer) with measurements of cell area, speed and direction were
42 obtained for each cell/track and timepoint. Cells were not selected for tracking if they were in
43 proximity to other cells of a distance of 35 μm . The measurements and object data were exported
44 and further analysis was performed. Data for each track included total length (timepoints),

1 speed(μm/s), Straightness, accumulated distance (μm), lateral displacement (μm) and vertical
2 displacement (μm).

3 *Data analysis.* This data was then analysed using an in-house script using Python library Pandas.
4 Tracks were discarded if they were less than 3 time-points in length. Means and Standard Deviations
5 were calculated for track length (timepoints), Speed (μm/s), Track Straightness and accumulated
6 distance. For each track the Parallel FMI (forward motion index) was calculated by taking a ratio of
7 vertical displacement to accumulated distance. The means and standard deviations for these were
8 calculated and reported for each condition similarly. Track Straightness is calculated as the ratio of
9 total displacement over total track length. Accumulated distance is the total length of the track from
10 the first to last time point of the track.

11 ***Clinical samples***

12 *Patients enrollment.* The study was approved by the Local Ethical committee of the Research
13 Institute for Complex Issues of Cardiovascular Diseases (Kemerovo, Russia, protocol number
14 20200212, dates of approval: 12 February 2020), and a written informed consent was provided by all
15 study participants after receiving a full explanation of the study. The investigation was carried out in
16 accordance with the Good Clinical Practice and the Declaration of Helsinki. Criteria of inclusion were:
17 1) performance of carotid endarterectomy due to chronic brain ischemia or ischemic stroke; 2) a
18 signed written informed consent to be enrolled. A criterion of exclusion was incomplete
19 investigation regardless of the reason; in this case, we enrolled another subject with similar age,
20 gender and clinicopathological features who met the inclusion criteria. Cerebrovascular disease
21 (chronic brain ischemia and ischemic stroke) as well as comorbid conditions (arterial hypertension,
22 chronic heart failure, chronic obstructive pulmonary disease, asthma, chronic kidney disease,
23 diabetes mellitus, overweight and obesity) were diagnosed and treated according to the respective
24 guidelines of European Society of Cardiology, Global Initiative for Chronic Obstructive Lung Disease,
25 Global Initiative for Asthma, Kidney Disease: Improving Global Outcomes, American Diabetes
26 Association, and European Association for the Study of Obesity. eGFR was calculated according to
27 the Chronic Kidney Disease Epidemiology Collaboration (CKD-EPI) equation. Extracranial artery
28 stenosis was assessed using the color duplex screening (Vivid 7 Dimension Ultrasound System,
29 General Electric Healthcare). Data on age, gender, smoking status and pharmacological anamnesis
30 were collected at the time of admission. In total, we enrolled 20 patients. The detailed
31 characteristics of the study samples are presented in Table S1.

32 *Sample collection and preparation.* Carotid atherosclerotic plaques (n = 14) and adjacent intact
33 arterial segments (n = 14) were pairwise excised during the carotid endarterectomy and divided into
34 3 segments each. The first segment was snap-frozen in the optimal cutting temperature compound
35 (Tissue-Tek, 4583, Sakura) using a liquid nitrogen and was then sectioned on a cryostat (Microm
36 HM525, 387779, Thermo Scientific). To ensure the proper immunofluorescence examination, we
37 prepared 8 sections (7μm thickness), evenly distributed across the entire carotid artery segment, per
38 slide. The second and third segments were homogenised in TRIzol Reagent (15596018, Thermo
39 Fisher Scientific) for RNA extraction or in T-PER Tissue Protein Extraction Reagent (78510, Thermo
40 Fisher Scientific) supplied with Halt protease and phosphatase inhibitor cocktail (78444, Thermo
41 Fisher Scientific) for the total protein extraction according to the manufacturer's protocols.
42 Quantification and quality control of the isolated RNA was performed employing Qubit 4
43 fluorometer (Q33238, Thermo Fisher Scientific), Qubit RNA BR assay kit (Q10210, Thermo Fisher
44 Scientific), Qubit RNA IQ assay kit (Q33222, Thermo Fisher Scientific), Qubit RNA IQ standards for
45 calibration (Q33235, Thermo Fisher Scientific) and Qubit assay tubes (Q32856, Thermo Fisher
46 Scientific) according to the manufacturer's protocols. Quantification of total protein was conducted

1 using BCA Protein Assay Kit (23227, Thermo Fisher Scientific) and Multiskan Sky microplate
2 spectrophotometer (51119700DP, Thermo Fisher Scientific) in accordance with the manufacturer's
3 protocol.

4 *Immunofluorescence examination.* Upon the sectioning, vascular tissues were dried at room
5 temperature for 30min, fixed and permeabilised in ice-cold acetone for 10min, incubated in 1%
6 bovine serum albumin (Cat. No. A2153, Sigma-Aldrich) for 1h to block non-specific protein binding,
7 stained with unconjugated mouse anti-human CD81 (M38 clone, NBP1-44861, 1:100, Novus
8 Biologicals) and rabbit anti-human fibronectin (F14 clone, ab45688, 1:250, Abcam) primary
9 antibodies and incubated at 4°C for 16h. Sections were further treated with pre-adsorbed donkey
10 anti-mouse Alexa Fluor 488-conjugated (ab150109, 1:500, Abcam) and donkey anti-rabbit Alexa
11 Fluor 555-conjugated secondary antibodies (ab150062, 1:500, Abcam) and incubated for 1h at room
12 temperature. Between all steps, washing was performed thrice with PBS (pH 7.4, P4417, Sigma-
13 Aldrich). Nuclei were counterstained with 4,6-diamidino-2-phenylindole (DAPI) for 30min at room
14 temperature (10µg/mL, D9542, Sigma-Aldrich). Coverslips were mounted with ProLong Gold
15 Antifade (P36934, Thermo Fisher Scientific). Sections were examined by confocal laser scanning
16 microscopy (LSM 700, Carl Zeiss). Colocalization analysis (n=12 images) was performed using the
17 respective ImageJ (National Institutes of Health) plugins (Colocalisation Threshold and Coloc2). To
18 evaluate the colocalization, we calculated Pearson's r above threshold (zero-zero pixels),
19 thresholded Mander's split colocalisation coefficient (the proportion of signal in each channel that
20 colocalizes with the other channel) for both (red and green) channels, percent volume colocalised
21 with each channel, and intensity volume above threshold colocalised with each channel in both
22 neointima and media.

23 *Reverse transcription-quantitative polymerase chain reaction (RT-qPCR).* Reverse transcription was
24 carried out utilising High Capacity cDNA Reverse Transcription Kit (4368814, Thermo Fisher
25 Scientific). Gene expression was measured by RT-qPCR using the customised primers (500nmol/L
26 each, Evrogen, Moscow, Russian Federation, Table S5), cDNA (20ng) and PowerUp SYBR Green
27 Master Mix (A25778, Thermo Fisher Scientific) according to the manufacturer's protocol for $T_m \geq$
28 60°C (fast cycling mode). Technical replicates (n=3 per each sample collected from one vascular
29 segment) were performed in all RT-qPCR experiments. The reaction was considered successful if its
30 efficiency was 90-105% and R^2 was ≥ 0.98 . Quantification of the *CD9*, *CD63*, *CD81*, *COL6A3*, *EDIL3*,
31 *CSPG4*, *TGFBI*, *FN1*, and *MYADM* mRNA levels in carotid atherosclerotic plaques (n=5) and adjacent
32 intact arterial segments (n = 5) was performed by using the $2^{-\Delta\Delta Ct}$ method. Relative transcript levels
33 were expressed as a value relative to the average of 3 housekeeping genes (*ACTB*, *GAPDH*, *B2M*).

34 *Western blotting.* Equal amounts of protein lysate (15µg per sample) of carotid atherosclerotic
35 plaques (n=12), adjacent intact arterial segments (n=12), and plaque-derived sEVs (n=6) were mixed
36 with NuPAGE lithium dodecyl sulfate sample buffer (NP0007, Thermo Fisher Scientific) at a 4:1 ratio
37 and NuPAGE sample reducing agent (NP0009, Thermo Fisher Scientific) at a 10:1 ratio, denatured at
38 99°C for 5 minutes, and then loaded on a 1.5mm NuPAGE 4-12% Bis-Tris protein gel (NP0335BOX,
39 Thermo Fisher Scientific). The 1:1 mixture of Novex Sharp pre-stained protein standard (LC5800,
40 Thermo Fisher Scientific) and MagicMark XP Western protein standard (LC5602, Thermo Fisher
41 Scientific) was loaded as a molecular weight marker. Proteins were separated by the sodium dodecyl
42 sulphate-polyacrylamide gel electrophoresis (SDS-PAGE) at 150V for 2h using NuPAGE 2-(N-
43 morpholino)ethanesulfonic acid SDS running buffer (NP0002, Thermo Fisher Scientific), NuPAGE
44 Antioxidant (NP0005, Thermo Fisher Scientific), and XCell SureLock Mini-Cell vertical mini-protein gel
45 electrophoresis system (E10001, Thermo Fisher Scientific). Protein transfer was performed using
46 polyvinylidene difluoride (PVDF) transfer stacks (IB24001, Thermo Fisher Scientific) and iBlot 2 Gel

1 Transfer Device (IB21001, Thermo Fisher Scientific) according to the manufacturer's protocols using
2 a standard transfer mode for 30-150 kDa proteins (P0 – 20 V for 1min, 23 V for 4min, and 25 V for 2
3 min). PVDF membranes were then incubated in iBind Flex Solution (SLF2020, Thermo Fisher
4 Scientific) for 1h to prevent non-specific binding.

5 Blots were probed with rabbit primary antibodies to CD9, fibronectin or CD81, and GAPDH (loading
6 control). Horseradish peroxidase-conjugated goat anti-rabbit (7074, Cell Signaling Technology) or
7 goat anti-mouse (AP130P, Sigma-Aldrich) secondary antibodies were used at 1:200 and 1:1000
8 dilution, respectively. Incubation with the antibodies was performed using iBind Flex Solution Kit
9 (SLF2020, Thermo Fisher Scientific), iBind Flex Cards (SLF2010, Thermo Fisher Scientific) and iBind
10 Flex Western Device (SLF2000, Thermo Fisher Scientific) during 3h according to the manufacturer's
11 protocols. Chemiluminescent detection was performed using SuperSignal West Pico PLUS
12 chemiluminescent substrate (34580, Thermo Fisher Scientific) and C-DiGit blot scanner (3600-00, LI-
13 COR Biosciences) in a high-sensitivity mode (12min scanning). Densitometry was performed using
14 the ImageJ software (National Institutes of Health) using the standard algorithm (consecutive
15 selection and plotting of the lanes with the measurement of the peak area) and subsequent
16 adjustment to the loading control (GAPDH).

17 **Statistics**

18 Data were analysed using GraphPad Prism (version 8.4.3). CD63-beads assay, NanoView, adhesion
19 assay, FA quantification were analysed by one-way ANOVA test. Two group CD63-bead assay was
20 analysed by non-paired T-test. 2D migration multiple comparison data and VSMC invasion multiple
21 comparison data were analysed using non-parametric Kruskal-Wallis test. Two group invasion data
22 were analysed using non-parametric Kolmogorov-Smirnov test. Clinical data for two groups was
23 analysed by non-paired T-test and multiple comparison was analysed by Mann-Whitney U-test. All
24 analysis was conducted using PRISM software (GraphPad, San Diego, CA). Values of P<0.05 were
25 considered statistically significant.

26 **Short abbreviations**

27 ECM extracellular matrix

28 EM electron microscopy

29 FN fibronectin

30 MVB multivesicular body

31 NTA nanoparticle tracking analysis

32 SMPD3 sphingomyelin phosphodiesterase 3

33 VSMC vascular smooth muscle cell

34

35

36

1 **Acknowledgments**

2 ANK and CS were supported by BHF-PG/17/37/33023. TI was supported by BHF PG/20/6/34835 and
3 FS/14/30/30917. REC was supported by National Institutes of General Medical Sciences grant
4 R01GM134531. AK, MS and LB were supported by the Ministry of Science and Higher Education of
5 the Russian Federation-Complex Program of Basic Research under the Siberian Branch of the Russian
6 Academy of Sciences within the Basic Research Topic of Research Institute for Complex Issues
7 of Cardiovascular Diseases № 0419-2021-001. We are thankful to Dr Adam A Walters for the flow
8 cytometry consultancy and help.

9 **Competing interests**

10 A. Kapustin is currently an employee and shareholder of AstraZeneca.

1 **References**

- 2 1. Libby, P., Ridker, P.M. & Hansson, G.K. Progress and challenges in translating the biology of
3 atherosclerosis. *Nature* **473**, 317-325 (2011).
- 4 2. Chappell, J. *et al.* Extensive Proliferation of a Subset of Differentiated, yet Plastic, Medial
5 Vascular Smooth Muscle Cells Contributes to Neointimal Formation in Mouse Injury and
6 Atherosclerosis Models. *Circ Res* **119**, 1313-1323 (2016).
- 7 3. Misra, A. *et al.* Integrin beta3 regulates clonality and fate of smooth muscle-derived
8 atherosclerotic plaque cells. *Nat Commun* **9**, 2073 (2018).
- 9 4. Durham, A.L., Speer, M.Y., Scatena, M., Giachelli, C.M. & Shanahan, C.M. Role of smooth
10 muscle cells in vascular calcification: implications in atherosclerosis and arterial stiffness.
Cardiovasc Res **114**, 590-600 (2018).
- 12 5. Rohwedder, I. *et al.* Plasma fibronectin deficiency impedes atherosclerosis progression and
13 fibrous cap formation. *EMBO Mol Med* **4**, 564-576 (2012).
- 14 6. Langley, S.R. *et al.* Extracellular matrix proteomics identifies molecular signature of
15 symptomatic carotid plaques. *J Clin Invest* **127**, 1546-1560 (2017).
- 16 7. Glukhova, M.A. *et al.* Expression of extra domain A fibronectin sequence in vascular smooth
17 muscle cells is phenotype dependent. *J Cell Biol* **109**, 357-366 (1989).
- 18 8. Pankov, R. & Yamada, K.M. Fibronectin at a glance. *J Cell Sci* **115**, 3861-3863 (2002).
- 19 9. Hocking, D.C., Sottile, J. & McKeown-Longo, P.J. Activation of distinct alpha5beta1-mediated
20 signaling pathways by fibronectin's cell adhesion and matrix assembly domains. *J Cell Biol*
141, 241-253 (1998).
- 22 10. Bass, M.D. *et al.* Syndecan-4-dependent Rac1 regulation determines directional migration in
23 response to the extracellular matrix. *J Cell Biol* **177**, 527-538 (2007).
- 24 11. Nobes, C.D. & Hall, A. Rho, rac, and cdc42 GTPases regulate the assembly of multimolecular
25 focal complexes associated with actin stress fibers, lamellipodia, and filopodia. *Cell* **81**, 53-62
(1995).
- 27 12. Sheetz, M.P., Felsenfeld, D.P. & Galbraith, C.G. Cell migration: regulation of force on
28 extracellular-matrix-integrin complexes. *Trends Cell Biol* **8**, 51-54 (1998).
- 29 13. Ridley, A.J. Rho GTPases and cell migration. *J Cell Sci* **114**, 2713-2722 (2001).
- 30 14. Sung, B.H., Ketova, T., Hoshino, D., Zijlstra, A. & Weaver, A.M. Directional cell movement
31 through tissues is controlled by exosome secretion. *Nat Commun* **6**, 7164 (2015).
- 32 15. Sung, B.H. & Weaver, A.M. Exosome secretion promotes chemotaxis of cancer cells. *Cell Adh
33 Migr* **11**, 187-195 (2017).
- 34 16. Sung, B.H. *et al.* A live cell reporter of exosome secretion and uptake reveals pathfinding
35 behavior of migrating cells. *Nat Commun* **11**, 2092 (2020).
- 36 17. Koumangoye, R.B., Sakwe, A.M., Goodwin, J.S., Patel, T. & Ochieng, J. Detachment of breast
37 tumor cells induces rapid secretion of exosomes which subsequently mediate cellular
38 adhesion and spreading. *PLoS One* **6**, e24234 (2011).
- 39 18. Hoshino, D. *et al.* Exosome secretion is enhanced by invadopodia and drives invasive
40 behavior. *Cell Rep* **5**, 1159-1168 (2013).
- 41 19. Clayton, A. *et al.* Adhesion and signaling by B cell-derived exosomes: the role of integrins.
FASEB J **18**, 977-979 (2004).
- 43 20. Brown, M. *et al.* Lymphatic exosomes promote dendritic cell migration along guidance cues.
J Cell Biol **217**, 2205-2221 (2018).
- 45 21. Majumdar, R., Tavakoli Tameh, A. & Parent, C.A. Exosomes Mediate LTB4 Release during
46 Neutrophil Chemotaxis. *PLoS Biol* **14**, e1002336 (2016).
- 47 22. Kriebel, P.W. *et al.* Extracellular vesicles direct migration by synthesizing and releasing
48 chemotactic signals. *J Cell Biol* **217**, 2891-2910 (2018).
- 49 23. Kapustin, A.N. *et al.* Vascular smooth muscle cell calcification is mediated by regulated
50 exosome secretion. *Circ Res* **116**, 1312-1323 (2015).

1 24. Beacham, D.A., Amatangelo, M.D. & Cukierman, E. Preparation of extracellular matrices
2 produced by cultured and primary fibroblasts. *Curr Protoc Cell Biol Chapter 10*, Unit 10 19
3 (2007).

4 25. Kowal, J. *et al.* Proteomic comparison defines novel markers to characterize heterogeneous
5 populations of extracellular vesicle subtypes. *Proc Natl Acad Sci U S A* **113**, E968-977 (2016).

6 26. Trajkovic, K. *et al.* Ceramide triggers budding of exosome vesicles into multivesicular
7 endosomes. *Science* **319**, 1244-1247 (2008).

8 27. Klinghoffer, R.A., Sachsenmaier, C., Cooper, J.A. & Soriano, P. Src family kinases are required
9 for integrin but not PDGFR signal transduction. *EMBO J* **18**, 2459-2471 (1999).

10 28. Sinha, S. *et al.* Cortactin promotes exosome secretion by controlling branched actin
11 dynamics. *J Cell Biol* **214**, 197-213 (2016).

12 29. Ruiz-Navarro, J. *et al.* Formin-like 1beta phosphorylation at S1086 is necessary for secretory
13 polarized traffic of exosomes at the immune synapse in Jurkat T lymphocytes. *Elife* **13**
14 (2024).

15 30. Campellone, K.G., Lebek, N.M. & King, V.L. Branching out in different directions: Emerging
16 cellular functions for the Arp2/3 complex and WASP-family actin nucleation factors. *Eur J
17 Cell Biol* **102**, 151301 (2023).

18 31. Nolen, B.J. *et al.* Characterization of two classes of small molecule inhibitors of Arp2/3
19 complex. *Nature* **460**, 1031-1034 (2009).

20 32. Rizvi, S.A. *et al.* Identification and characterization of a small molecule inhibitor of formin-
21 mediated actin assembly. *Chem Biol* **16**, 1158-1168 (2009).

22 33. Taunton, J. *et al.* Actin-dependent propulsion of endosomes and lysosomes by recruitment
23 of N-WASP. *J Cell Biol* **148**, 519-530 (2000).

24 34. Abella, J.V. *et al.* Isoform diversity in the Arp2/3 complex determines actin filament
25 dynamics. *Nat Cell Biol* **18**, 76-86 (2016).

26 35. Thomas, S., Popov, V.L. & Walker, D.H. Exit mechanisms of the intracellular bacterium
27 Ehrlichia. *PLoS One* **5**, e15775 (2010).

28 36. Mellor, H. The role of formins in filopodia formation. *Biochim Biophys Acta* **1803**, 191-200
29 (2010).

30 37. Bohil, A.B., Robertson, B.W. & Cheney, R.E. Myosin-X is a molecular motor that functions in
31 filopodia formation. *Proc Natl Acad Sci U S A* **103**, 12411-12416 (2006).

32 38. Heusermann, W. *et al.* Exosomes surf on filopodia to enter cells at endocytic hot spots,
33 traffic within endosomes, and are targeted to the ER. *J Cell Biol* **213**, 173-184 (2016).

34 39. Verweij, F.J. *et al.* Quantifying exosome secretion from single cells reveals a modulatory role
35 for GPCR signaling. *J Cell Biol* **217**, 1129-1142 (2018).

36 40. Hutcheson, J.D. *et al.* Genesis and growth of extracellular-vesicle-derived microcalcification
37 in atherosclerotic plaques. *Nat Mater* **15**, 335-343 (2016).

38 41. Whitehead, M. *et al.* Vascular smooth muscle cell senescence accelerates medin aggregation
39 via small extracellular vesicle secretion and extracellular matrix reorganization. *Aging Cell*
40 **22**, e13746 (2023).

41 42. Didangelos, A. *et al.* Proteomics characterization of extracellular space components in the
42 human aorta. *Mol Cell Proteomics* **9**, 2048-2062 (2010).

43 43. Kapustin, A.N. *et al.* Prothrombin Loading of Vascular Smooth Muscle Cell-Derived Exosomes
44 Regulates Coagulation and Calcification. *Arterioscler Thromb Vasc Biol* **37**, e22-e32 (2017).

45 44. Tagliatela, A.C. *et al.* Coronin 1C inhibits melanoma metastasis through regulation of MT1-
46 MMP-containing extracellular vesicle secretion. *Sci Rep* **10**, 11958 (2020).

47 45. Rohlena, J. *et al.* Endothelial CD81 is a marker of early human atherosclerotic plaques and
48 facilitates monocyte adhesion. *Cardiovasc Res* **81**, 187-196 (2009).

49 46. Burridge, K. Foot in mouth: do focal adhesions disassemble by endocytosis? *Nat Cell Biol* **7**,
50 545-547 (2005).

1 47. Holt, M.R. *et al.* Quantifying cell-matrix adhesion dynamics in living cells using interference
2 reflection microscopy. *J Microsc* **232**, 73-81 (2008).

3 48. Chrzanowska-Wodnicka, M. & Burridge, K. Rho-stimulated contractility drives the formation
4 of stress fibers and focal adhesions. *J Cell Biol* **133**, 1403-1415 (1996).

5 49. Arthur, W.T. & Burridge, K. RhoA inactivation by p190RhoGAP regulates cell spreading and
6 migration by promoting membrane protrusion and polarity. *Mol Biol Cell* **12**, 2711-2720
7 (2001).

8 50. Tabdanov, E. *et al.* Micropatterning of TCR and LFA-1 ligands reveals complementary effects
9 on cytoskeleton mechanics in T cells. *Integr Biol (Camb)* **7**, 1272-1284 (2015).

10 51. Schoen, I., Hu, W., Klotzsch, E. & Vogel, V. Probing cellular traction forces by micropillar
11 arrays: contribution of substrate warping to pillar deflection. *Nano Lett* **10**, 1823-1830
12 (2010).

13 52. Ghibaudo, M. *et al.* Traction forces and rigidity sensing regulate cell functions *Soft Matter* **4**,
14 1836-1843 (2008).

15 53. Tillet, E., Gentil, B., Garrone, R. & Stallcup, W.B. NG2 proteoglycan mediates beta1 integrin-
16 independent cell adhesion and spreading on collagen VI. *J Cell Biochem* **86**, 726-736 (2002).

17 54. Nishida, S. *et al.* Collagen VI suppresses fibronectin-induced enteric neural crest cell
18 migration by downregulation of focal adhesion proteins. *Biochem Biophys Res Commun* **495**,
19 1461-1467 (2018).

20 55. Sardone, F. *et al.* Collagen VI-NG2 axis in human tendon fibroblasts under conditions
21 mimicking injury response. *Matrix Biol* **55**, 90-105 (2016).

22 56. Pankova, K., Rosel, D., Novotny, M. & Brabek, J. The molecular mechanisms of transition
23 between mesenchymal and amoeboid invasiveness in tumor cells. *Cell Mol Life Sci* **67**, 63-71
24 (2010).

25 57. Galbraith, C.G., Yamada, K.M. & Galbraith, J.A. Polymerizing actin fibers position integrins
26 primed to probe for adhesion sites. *Science* **315**, 992-995 (2007).

27 58. Pollard, T.D. & Borisy, G.G. Cellular motility driven by assembly and disassembly of actin
28 filaments. *Cell* **112**, 453-465 (2003).

29 59. Ridley, A.J. & Hall, A. The small GTP-binding protein rho regulates the assembly of focal
30 adhesions and actin stress fibers in response to growth factors. *Cell* **70**, 389-399 (1992).

31 60. Price, L.S., Leng, J., Schwartz, M.A. & Bokoch, G.M. Activation of Rac and Cdc42 by integrins
32 mediates cell spreading. *Mol Biol Cell* **9**, 1863-1871 (1998).

33 61. Ren, X.D., Kiosses, W.B. & Schwartz, M.A. Regulation of the small GTP-binding protein Rho
34 by cell adhesion and the cytoskeleton. *EMBO J* **18**, 578-585 (1999).

35 62. Wang, H.R. *et al.* Regulation of cell polarity and protrusion formation by targeting RhoA for
36 degradation. *Science* **302**, 1775-1779 (2003).

37 63. Rottner, K., Hall, A. & Small, J.V. Interplay between Rac and Rho in the control of substrate
38 contact dynamics. *Curr Biol* **9**, 640-648 (1999).

39 64. Roberts, L.A., Glenn, H., Hahn, C.S. & Jacobson, B.S. Cdc42 and RhoA are differentially
40 regulated during arachidonate-mediated HeLa cell adhesion. *J Cell Physiol* **196**, 196-205
41 (2003).

42 65. Nobes, C.D. & Hall, A. Rho GTPases control polarity, protrusion, and adhesion during cell
43 movement. *J Cell Biol* **144**, 1235-1244 (1999).

44 66. Cox, E.A., Sastry, S.K. & Huttenlocher, A. Integrin-mediated adhesion regulates cell polarity
45 and membrane protrusion through the Rho family of GTPases. *Mol Biol Cell* **12**, 265-277
46 (2001).

47 67. Matera, D.L., Lee, A.T., Hiraki, H.L. & Baker, B.M. The Role of Rho GTPases During Fibroblast
48 Spreading, Migration, and Myofibroblast Differentiation in 3D Synthetic Fibrous Matrices.
49 *Cell Mol Bioeng* **14**, 381-396 (2021).

50 68. Sahai, E. & Marshall, C.J. Differing modes of tumour cell invasion have distinct requirements
51 for Rho/ROCK signalling and extracellular proteolysis. *Nat Cell Biol* **5**, 711-719 (2003).

1 69. Sanz-Moreno, V. *et al.* Rac activation and inactivation control plasticity of tumor cell
2 movement. *Cell* **135**, 510-523 (2008).

3 70. Okada, M. *et al.* Primary collagen VI deficiency is the second most common congenital
4 muscular dystrophy in Japan. *Neurology* **69**, 1035-1042 (2007).

5 71. Bryant, J.E. *et al.* Cardiac myofibroblast differentiation is attenuated by alpha(3) integrin
6 blockade: potential role in post-MI remodeling. *J Mol Cell Cardiol* **46**, 186-192 (2009).

7 72. Luther, D.J. *et al.* Absence of type VI collagen paradoxically improves cardiac function,
8 structure, and remodeling after myocardial infarction. *Circ Res* **110**, 851-856 (2012).

9 73. Katsuda, S. *et al.* Collagens in human atherosclerosis. Immunohistochemical analysis using
10 collagen type-specific antibodies. *Arterioscler Thromb* **12**, 494-502 (1992).

11 74. Liu, X. *et al.* Collagen VI antibody reduces atherosclerosis by activating
12 monocyte/macrophage polarization in ApoE(-/-) mice. *Int Immunopharmacol* **111**, 109100
13 (2022).

14 75. He, M. *et al.* Hepatocellular carcinoma-derived exosomes promote motility of immortalized
15 hepatocyte through transfer of oncogenic proteins and RNAs. *Carcinogenesis* **36**, 1008-1018
16 (2015).

17 76. Doane, K.J., Howell, S.J. & Birk, D.E. Identification and functional characterization of two type
18 VI collagen receptors, alpha 3 beta 1 integrin and NG2, during avian corneal stromal
19 development. *Invest Ophthalmol Vis Sci* **39**, 263-275 (1998).

20 77. Nishiyama, A. & Stallcup, W.B. Expression of NG2 proteoglycan causes retention of type VI
21 collagen on the cell surface. *Mol Biol Cell* **4**, 1097-1108 (1993).

22 78. Nanda, A. *et al.* TEM8 interacts with the cleaved C5 domain of collagen alpha 3(VI). *Cancer*
23 *Res* **64**, 817-820 (2004).

24 79. Burgi, J. *et al.* CMG2/ANTXR2 regulates extracellular collagen VI which accumulates in
25 hyaline fibromatosis syndrome. *Nat Commun* **8**, 15861 (2017).

26 80. Burgi, J. *et al.* Ligand Binding to the Collagen VI Receptor Triggers a Talin-to-RhoA Switch that
27 Regulates Receptor Endocytosis. *Dev Cell* **53**, 418-430 e414 (2020).

28 81. Pankova, D. *et al.* NG2-mediated Rho activation promotes amoeboid invasiveness of cancer
29 cells. *Eur J Cell Biol* **91**, 969-977 (2012).

30 82. She, Z.G. *et al.* NG2 Proteoglycan Ablation Reduces Foam Cell Formation and Atherogenesis
31 via Decreased Low-Density Lipoprotein Retention by Synthetic Smooth Muscle Cells.
32 *Arterioscler Thromb Vasc Biol* **36**, 49-59 (2016).

33 83. Holm Nielsen, S. *et al.* The novel collagen matrikine, endotrophin, is associated with
34 mortality and cardiovascular events in patients with atherosclerosis. *J Intern Med* **290**, 179-
35 189 (2021).

36 84. Frimodt-Møller, M. *et al.* A marker of type VI collagen formation (PRO-C6) is associated with
37 higher arterial stiffness in type 1 diabetes. *Acta Diabetol* **56**, 711-712 (2019).

38 85. Lee, J.E. *et al.* Identification of EDIL3 on extracellular vesicles involved in breast cancer cell
39 invasion. *J Proteomics* **131**, 17-28 (2016).

40 86. Costanza, B. *et al.* Transforming growth factor beta-induced, an extracellular matrix
41 interacting protein, enhances glycolysis and promotes pancreatic cancer cell migration. *Int J*
42 *Cancer* **145**, 1570-1584 (2019).

43 87. Stampolidis, P., Ullrich, A. & Iacobelli, S. LGALS3BP, lectin galactoside-binding soluble 3
44 binding protein, promotes oncogenic cellular events impeded by antibody intervention.
45 *Oncogene* **34**, 39-52 (2015).

46 88. Savina, A., Furlan, M., Vidal, M. & Colombo, M.I. Exosome release is regulated by a calcium-
47 dependent mechanism in K562 cells. *J Biol Chem* **278**, 20083-20090 (2003).

48 89. Jae, N., McEwan, D.G., Manavski, Y., Boon, R.A. & Dimmeler, S. Rab7a and Rab27b control
49 secretion of endothelial microRNA through extracellular vesicles. *FEBS Lett* **589**, 3182-3188
50 (2015).

1 90. Savina, A., Vidal, M. & Colombo, M.I. The exosome pathway in K562 cells is regulated by
2 Rab11. *J Cell Sci* **115**, 2505-2515 (2002).

3 91. Baietti, M.F. *et al.* Syndecan-syntenin-ALIX regulates the biogenesis of exosomes. *Nat Cell*
4 *Biol* **14**, 677-685 (2012).

5 92. Goetsch, C. *et al.* Sortilin mediates vascular calcification via its recruitment into extracellular
6 vesicles. *J Clin Invest* **126**, 1323-1336 (2016).

7 93. van Niel, G. *et al.* The tetraspanin CD63 regulates ESCRT-independent and -dependent
8 endosomal sorting during melanogenesis. *Dev Cell* **21**, 708-721 (2011).

9 94. Pickering, J.G. *et al.* alpha5beta1 integrin expression and luminal edge fibronectin matrix
10 assembly by smooth muscle cells after arterial injury. *Am J Pathol* **156**, 453-465 (2000).

11 95. Slepian, M.J., Massia, S.P., Dehdashti, B., Fritz, A. & Whitesell, L. Beta3-integrins rather than
12 beta1-integrins dominate integrin-matrix interactions involved in postinjury smooth muscle
13 cell migration. *Circulation* **97**, 1818-1827 (1998).

14 96. Libby, P. & Aikawa, M. Stabilization of atherosclerotic plaques: new mechanisms and clinical
15 targets. *Nat Med* **8**, 1257-1262 (2002).

16 97. Parsons, M., Messent, A.J., Humphries, J.D., Deakin, N.O. & Humphries, M.J. Quantification
17 of integrin receptor agonism by fluorescence lifetime imaging. *J Cell Sci* **121**, 265-271 (2008).

18 98. Bampton, E.T.W., Goemans, C.G., Niranjan, D., Mizushima, N. & Tolkovsky, A.M. The
19 Dynamics of Autophagy Visualised in Live Cells: from Autophagosome Formation to Fusion
20 with Endo/lysosomes. *Autophagy* **1**, 23-36 (2005).

21 99. Leifer, C.A. *et al.* TLR9 is localized in the endoplasmic reticulum prior to stimulation. *J*
22 *Immunol* **173**, 1179-1183 (2004).

23 100. Berg, J.S. & Cheney, R.E. Myosin-X is an unconventional myosin that undergoes
24 intrafilopodial motility. *Nat Cell Biol* **4**, 246-250 (2002).

25 101. Reynolds, J.L. *et al.* Human vascular smooth muscle cells undergo vesicle-mediated
26 calcification in response to changes in extracellular calcium and phosphate concentrations: a
27 potential mechanism for accelerated vascular calcification in ESRD. *J Am Soc Nephrol* **15**,
28 2857-2867 (2004).

29 102. Kapustin, A.N. *et al.* Calcium regulates key components of vascular smooth muscle cell-
30 derived matrix vesicles to enhance mineralization. *Circ Res* **109**, e1-12 (2011).

31 103. Kapustin, A.N. *et al.* Antisense oligonucleotide activity in tumour cells is influenced by
32 intracellular LBPA distribution and extracellular vesicle recycling. *Communications Biology* **4**,
33 1241 (2021).

34 104. Pandey, P. *et al.* Cardiomyocytes Sense Matrix Rigidity through a Combination of Muscle and
35 Non-muscle Myosin Contractions. *Dev Cell* **45**, 661 (2018).

36

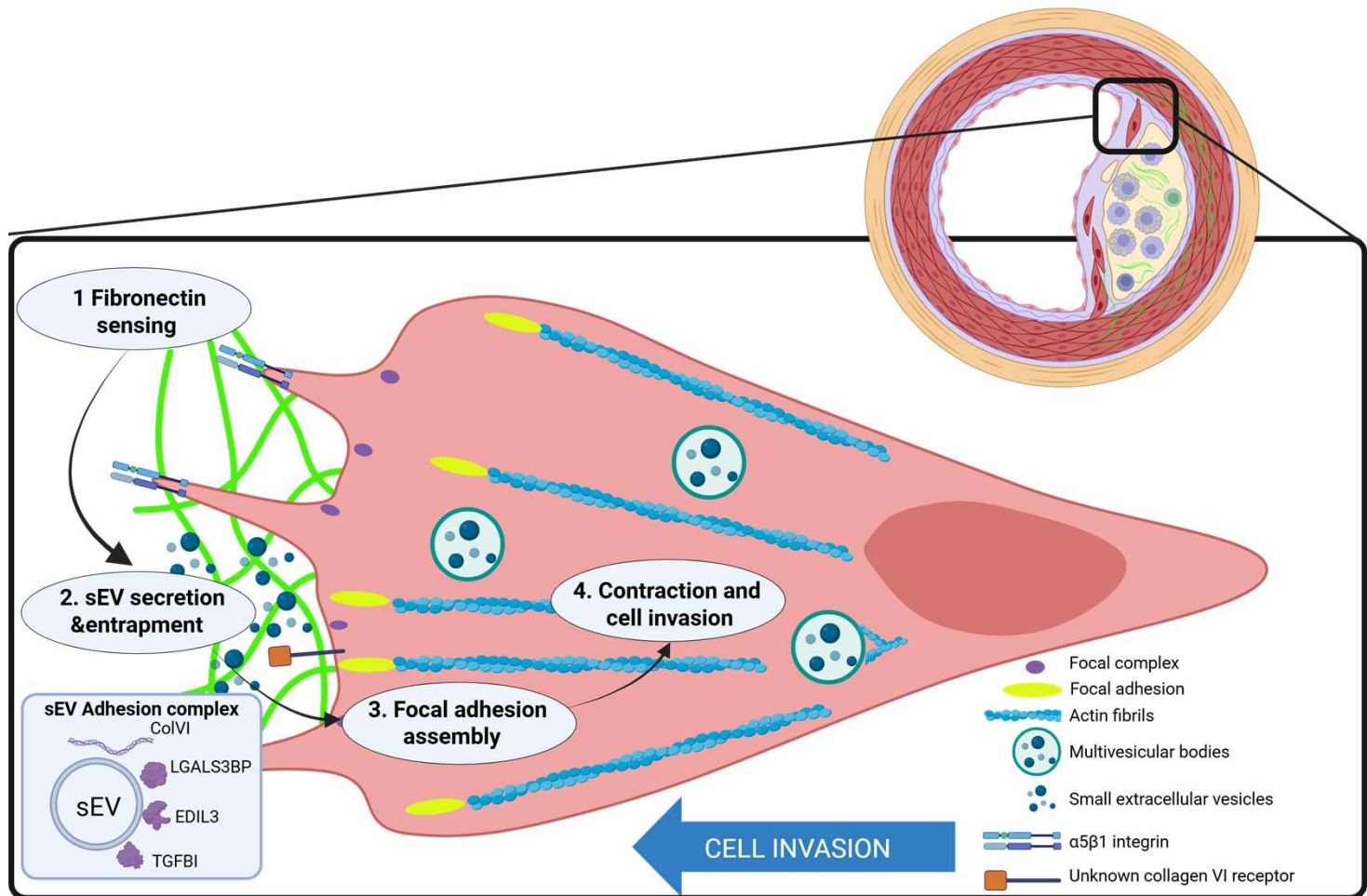
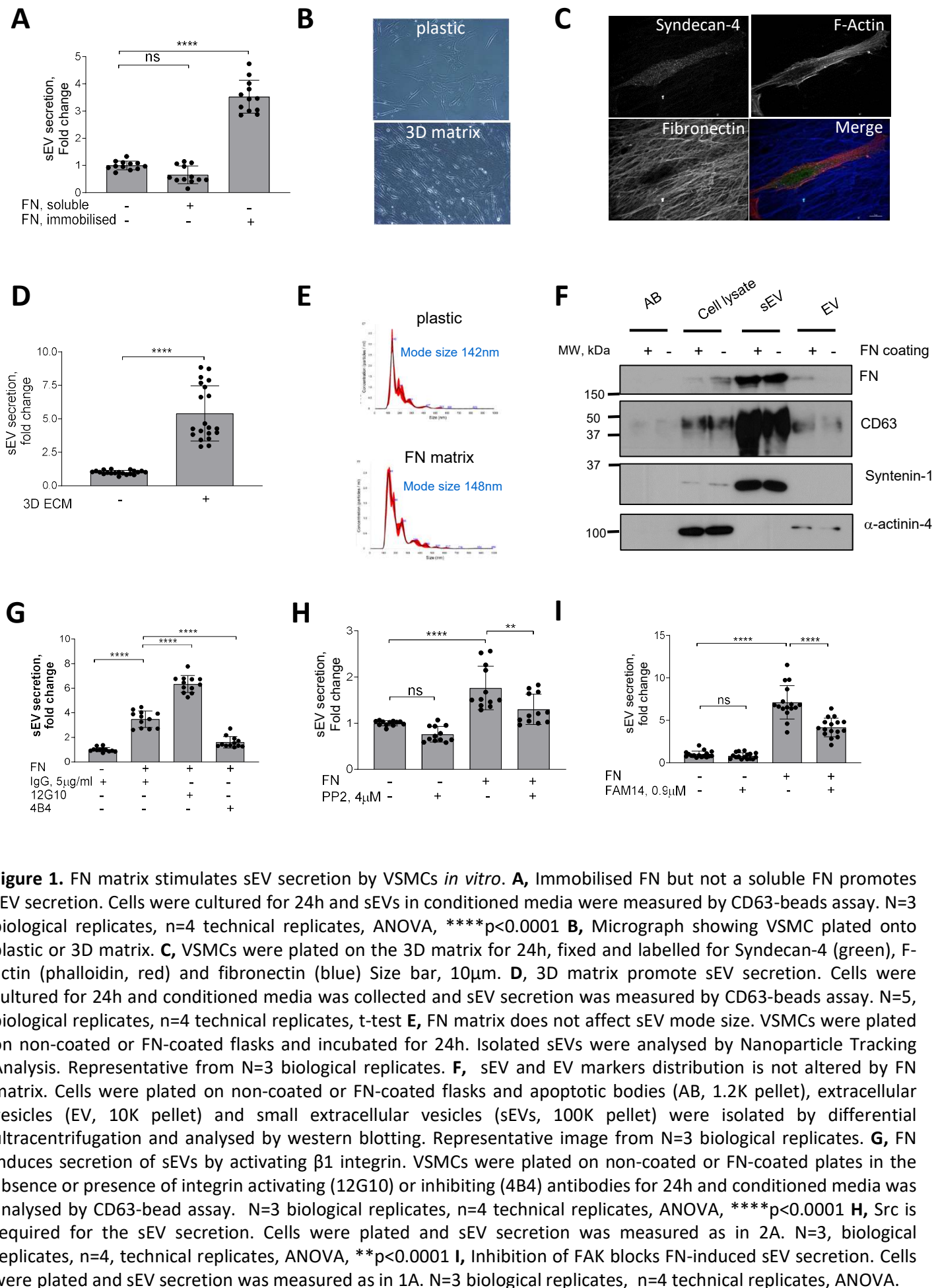


Figure Abstract

Vascular smooth muscle cells sense fibronectin via $\beta 1$ integrin and secrete small extracellular vesicles loaded with collagen VI. These extracellular vesicles are entrapped in the extracellular matrix and induce formation of peripheral focal adhesions presenting adhesion complex ECM proteins including collagen VI, LGALS3BP, EDIL3 and TGFBI. Focal adhesions anchor the extracellular matrix to actin fibrils in the cell. Contraction of the actin fibrils generates the mechanical force for directional cell invasion through the matrix. This figure was created with BioRender (<https://biorender.com/>).



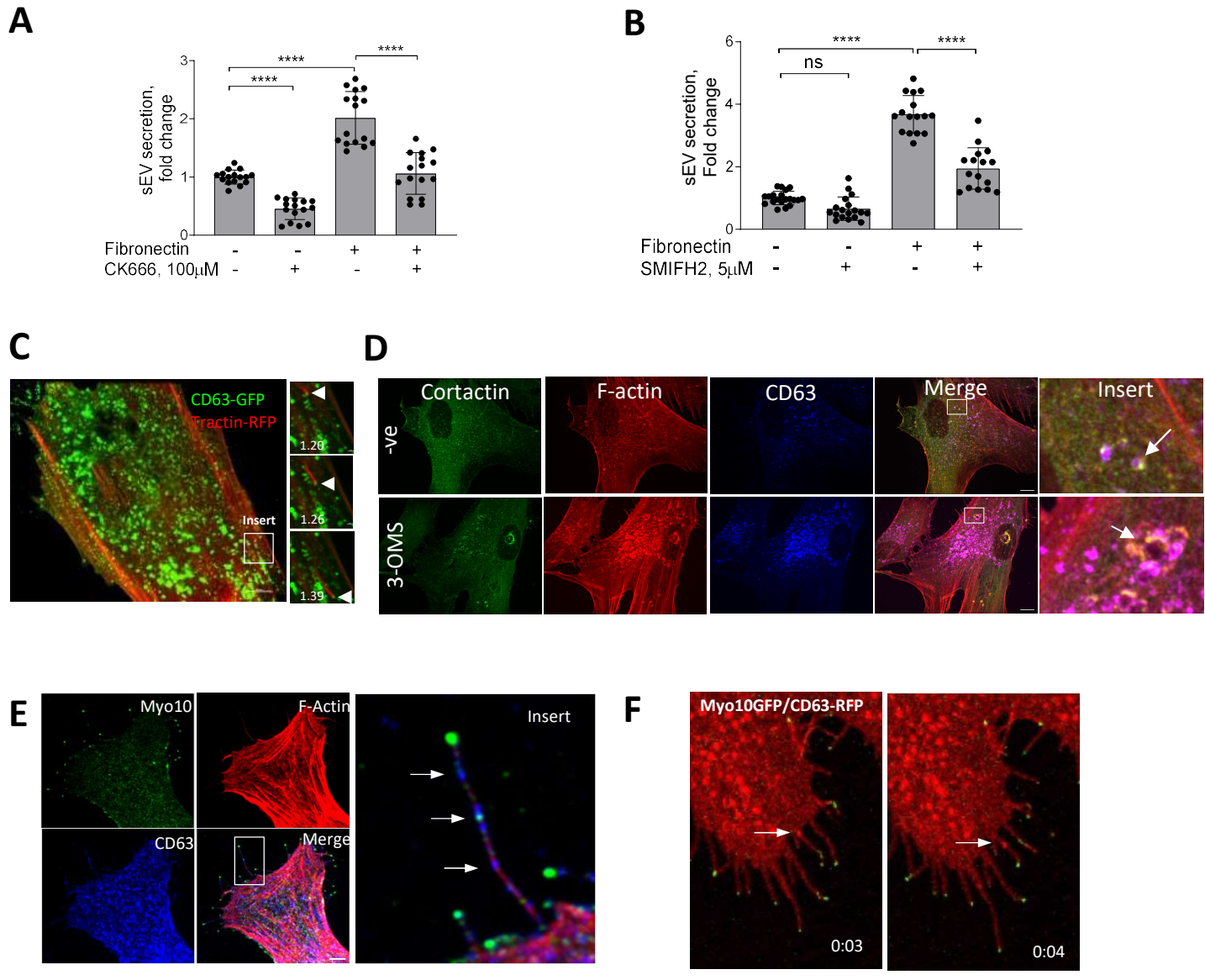


Figure 2. sEV secretion is regulated by Arp2/3 and formin-dependent actin cytoskeleton remodelling. **A**, Arp2/3 inhibition with CK666 reduces sEV secretion in VSMC. Cells were plated onto non-coated or FN-coated plates for 24h and conditioned media was analyzed by CD63-bead assay. N=4 biological replicates, n=4 technical replicates, ANOVA. **B**, Formin inhibitor, SMIFH2 blocking filopodia formation reduces sEV secretion from FN-plated cells only. Cells were plated onto non-coated or FN-coated plates for 24h and conditioned media was analyzed by CD63-bead assay. N=4-5 biological replicates, n=2-4 technical replicates, ANOVA. **C**, Still images of a time-lapse showing that transported MVBs are attached to F-actin tails. VSMCs were co-transfected with CD63-GFP and F-tractin-RFP and time-lapse was captured using confocal spinning-disk microscopy. Arrow head – position of CD63 MVB across time. Time, min. Size bar, 10μm. **D**, VSMC were plated for 24h in the absence (top, -ve) or presence of sEV secretion inhibitor (3-OMS, 10μM). Cells were fixed and stained for cortactin, F-actin and CD63. Note an overlap between CD63 endosomes and branched actin proteins (F-actin and cortactin), which is enhanced by 3-OMS treatment (arrow). Size bar, 10μm. **E**, CD63 MVBs (arrows) are detected in filopodia-like structures. VSMCs were plated on FN-coated plates for 24h and cells were stained for Myo10 (green), CD63 (blue), F-actin (phalloidin, red). Size bar, 10μm. **C**, Still images of a time-lapse showing that MVBs are transported to the filopodia tip in the live VSMC. Cells were co-transfected by CD63-RFP and Myo10-GFP, cultured for 24h and time-lapse video was captured using confocal spinning disk microscopy. Snapshots were taken at T=3s and T=4s after start of the video.

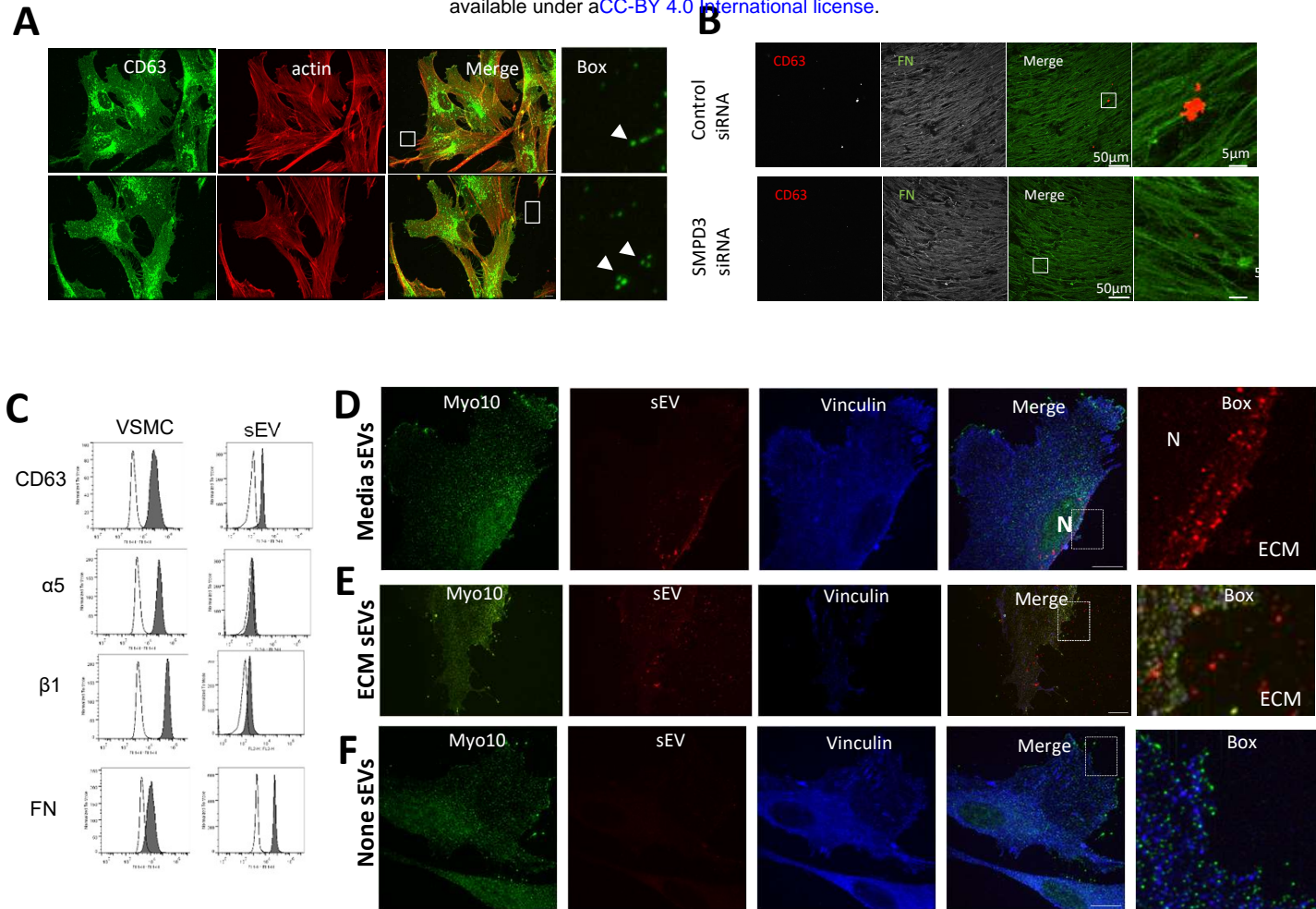


Figure 3. Endogenous and exogenous sEVs are trapped by ECM *in vitro*. **A**, VSMC were plated onto non-coated (top) or FN-coated (bottom) plastic for 24h and stained for the membrane sEV marker, CD63 and F-actin. Note accumulation of CD63 puncta in close proximity to filopodia-like projections. Size bar, 10μm. **B**, VSMCs were plated onto gelatin-coated plates and treated with control or SMPD3 siRNA for 72h. 3D matrices were generated and stained for CD63 and FN. Images were acquired using Nikon AX inverted confocal microscope. Note the decrease in CD63-positive sEVs associated with the FN fibrils. **C**, FN is presented on the surface of the VSMC-derived sEV along with α5β1 integrin. VSMC sEVs were immobilised on the 4μm beads. sEV-beads and VSMCs were stained with the antibodies (filled graphs) in non-permeabilised conditions and analysed by flow cytometry. **D**, VSMC were plated on FN-coated dishes and Alexa568-labelled sEV were added to the cell media for 3h. Cells were fixed and stained for filopodia marker Myo10 (green) and vinculin (blue). Note perinuclear localisation of internalised sEVs. Size bar, 10μm. Representative image from N=3 biological replicates. **E**, VSMC were plated on FN-coated dishes pre-coated with Alexa568-labelled sEV and incubated for 24h. Cell staining as in Fig 3D. Note even distribution of sEVs across the matrix and cell area. **F**, VSMC were plated on the FN-coated dishes in the absence of Alexa568-labelled sEV and incubated for 24h. Cell staining as in Fig 3D. Note the absence of signal in sEV channel.

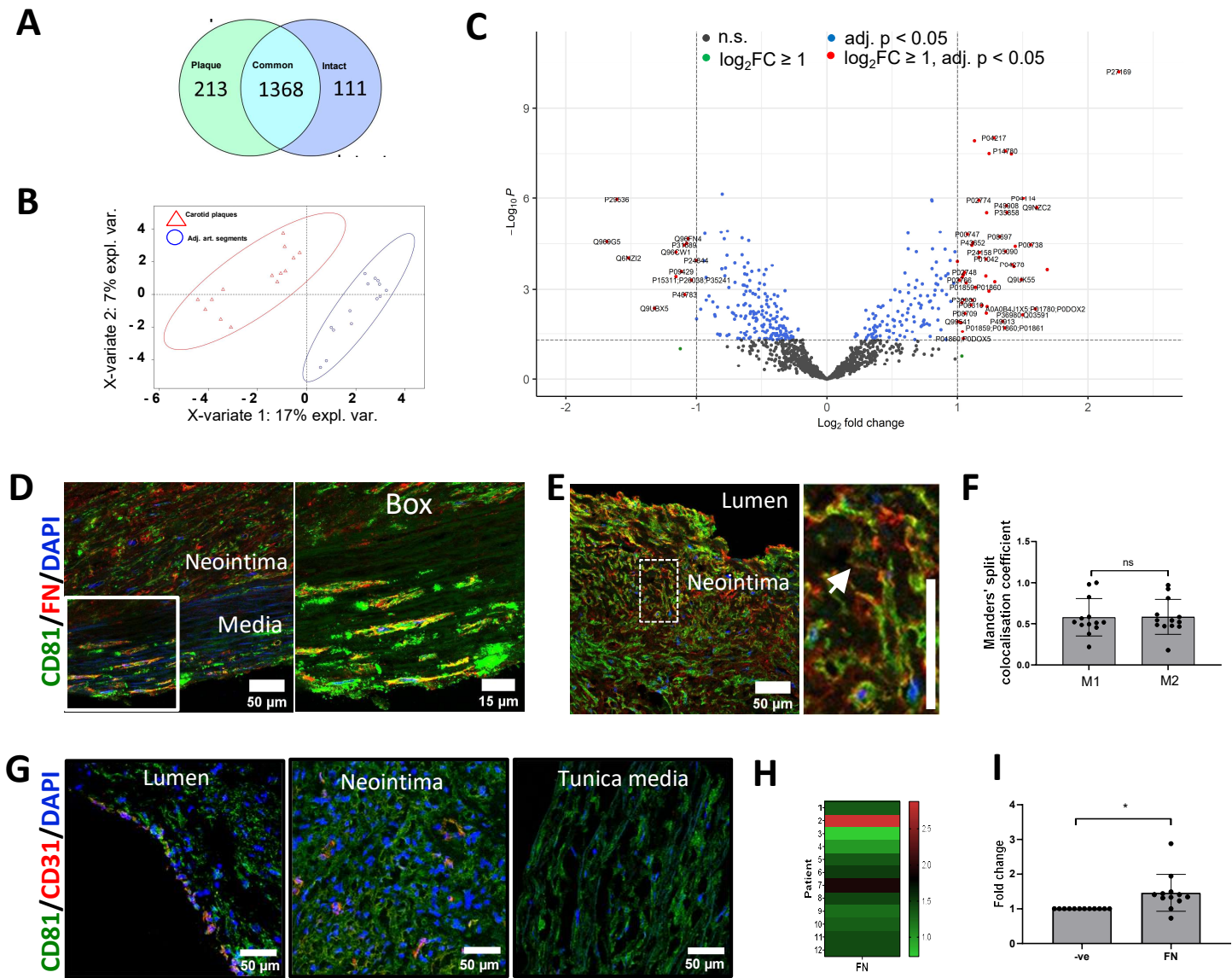


Figure 4. Fibronectin deposition in the atherosclerotic plaque is spatially associated with sEV markers.

A, Proteomic profiling of pairwise collected carotid atherosclerotic plaques and adjacent intact arterial segments. Venn diagram shows the number of plaque-specific ($n = 213$) and intact-specific ($n = 111$) proteins as well as the number of proteins which are common for both vascular regions (1,368). **B**, Partial least-squares discriminant analysis indicates clear classification pattern between the carotid plaques (indicated by red triangles) and adjacent intact arterial segments (indicated by blue circles). $N = 14$ patients. **C**, Volcano plot illustrates that 46 proteins are significantly overexpressed in plaques whilst 13 proteins are significantly upregulated in adjacent intact arterial segments. **D, E**, Atherosclerotic plaques were co-stained for fibronectin (FN) and sEV marker, CD81. Cell nuclei were counterstained with DAPI. Main figure: $\times 200$ magnification, size bar, 50 μm . Box: $\times 400$ magnification, size bar, 15 μm . Note an accumulation of FN in the neointima. **F**, Spatial distribution of FN and CD81 in the neointima. Note high overlap between FN and CD81 in the extracellular matrix. $\times 200$ magnification, size bar, 50 μm . Manders' split colocalization coefficient for the overlap of FN with CD81 (M1) and CD81 with FN (M2). Neointima region as in Fig. 4E. **G**, Co-localisation of endothelial cells (stained for CD31/PECAM1, red colour) and sEVs (stained for CD81, green colour). Nuclei are counterstained with 4',6-diamidino-2-phenylindole (DAPI, blue colour). Magnification: $\times 200$, scale bar: 50 μm . Note endothelialised (i.e., those covered with CD31-positive cells) segments at the luminal side and abundant CD81 expression both in the neointima and in the tunica media. Endothelial cells (CD31, red colour) are largely co-localised with CD81-positive extracellular vesicles (green colour). Note CD31-positive capillaries in the neointima. **H, I**, Quantification of FN content in atherosclerotic plaques. Samples were analysed by western blot and bands intensity was quantified in ImageJ. Fold change was calculated as ratio of band intensity in the atherosclerotic plaque to band intensity in the adjacent intact arterial segments normalised to GAPDH. Note that FN content is elevated in atherosclerotic plaques relative to the adjacent intact arterial segments. Paired t-test.

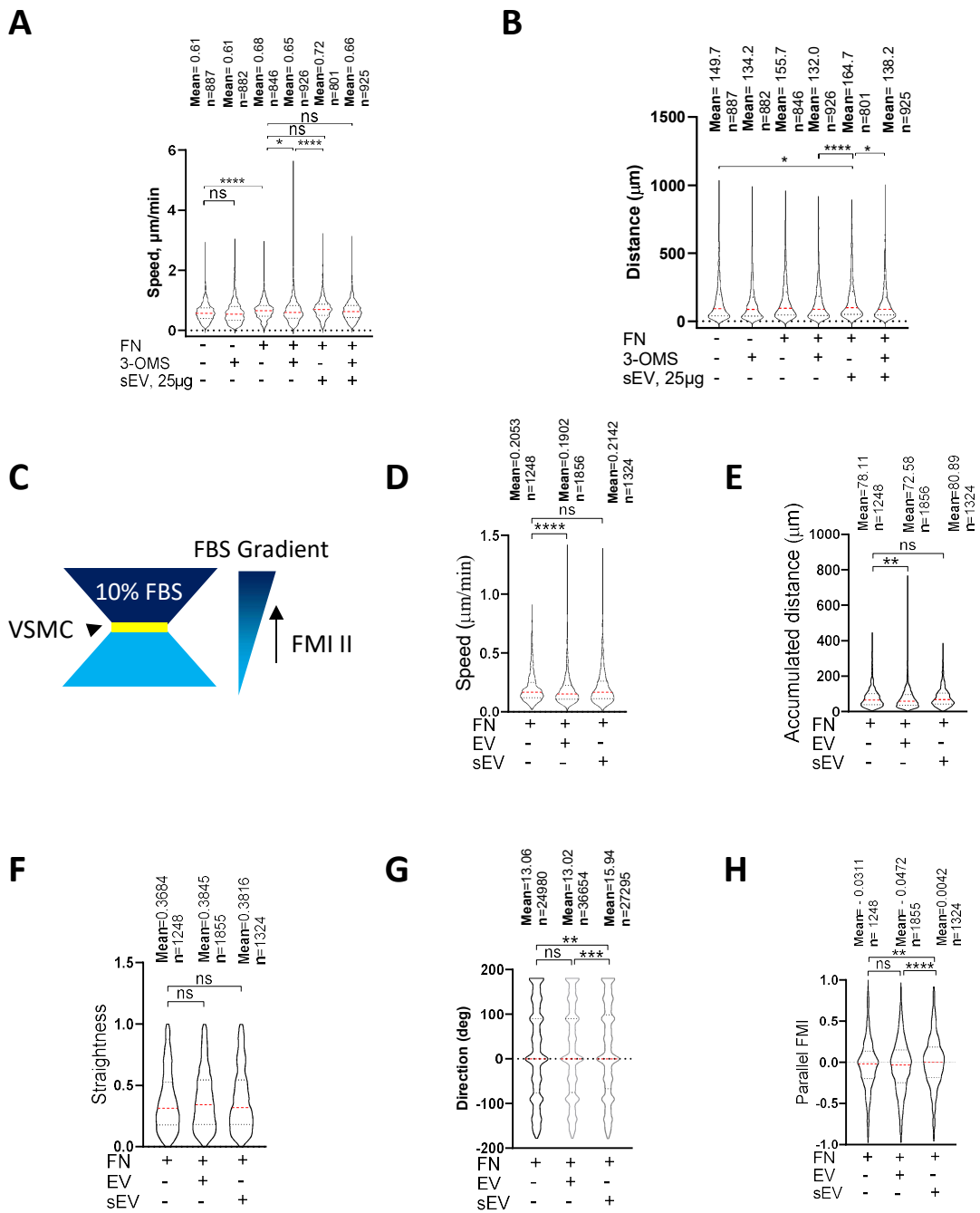


Figure 5. sEV induces directional VSMC invasion. **A, B**, VSMC migration in 2D assay. VSMC were plated onto FN in the absence or presence of SMPD3 inhibitor (3-OMS) and/or sEV (25 μg). Cells were tracked for 8h. Kruskal-Wallis with Dunn's multiple comparison test, N=2-3 biological replicates, n indicates the total number of tracked cells per condition, **, p<0.01, ****, p<0.0001. **C**, Chemotaxis μ-slide diagram. Yellow, cell chamber, blue chemoattractant-free medium chamber, dark blue – chemoattractant medium chamber. **D-H**, sEV promote directional VSMC invasion. Cells were seeded to the FN-enriched Matrigel matrix in μ-Slide Chemotaxis assay and stained with Draq5. Cell tracking was conducted by OperaPhenix microscope for 12h and cell invasion parameters were quantified using Columbus. Kruskal-Wallis with Dunn's multiple comparison test, N=4, biological replicates, n indicates the total number of tracked cells per condition, **, p<0.01, ***, p<0.001, ****, p<0.0001.

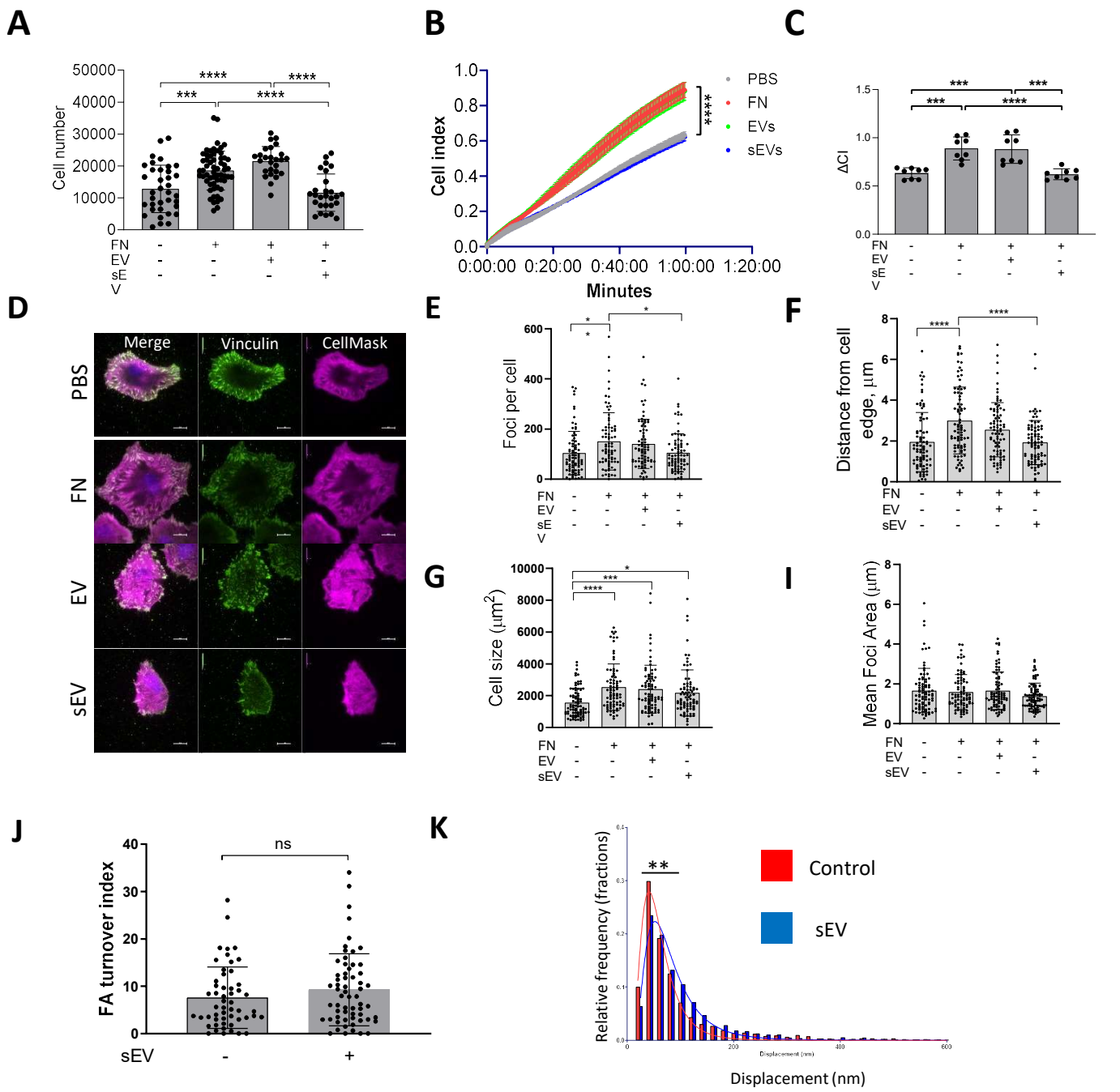


Figure 6. sEVs induce formation of peripheral FAs. **A**, VSMC were plated on FN matrix for 30min and adhered cells were counted by crystal violet staining. N=6 biological replicates, n=4-10 technical replicates, ANOVA, ***p<0.001, ****, p<0.0001 **B, C**, VSMC spreading onto FN was tracked by using ACEA's xCELLigence Real-Time Cell Analysis. Note that FN matrix promoted VSMC adhesion but addition of sEVs inhibited cell spreading. N=3 biological replicates, n=2-3 technical replicates, ANOVA. **D**, VSMCs were spread onto FN for 30 min and cells were fixed and stained with CellMask (magenta) and vinculin (green). Size bar, 10μm. **E, F, G, H**, Quantification of FA number, distance from plasma membrane, cell size and mean FA size per cell, respectively. FA were stained as in 5D and quantified. Representative data from N=3 biological replicates, n=80-82 total number of tracked cells per condition, ANOVA, *p<0.05, **p<0.01. **J**, Focal adhesion turnover is not affected by sEVs. VSMC were transfected with Paxillin-RFP and plated on the FN in the absence or presence of immobilised sEVs. Images were captured for 30min using confocal spinning disk microscopy and FA turnover was quantified using extracted images analysis, N=4, total n=53-61 cells per condition, Unpaired T-test. **K**, sEV induces formation of strong-pulling FAs. VSMC transfected with Paxillin-RFP were plated on the PDMS pillars which were covered with FN and sEVs and pillar displacements were quantified. **p<0.01, Unpaired t-test, Data represent 2,170-2322 measurements per condition pooled from two independent biological replicates.

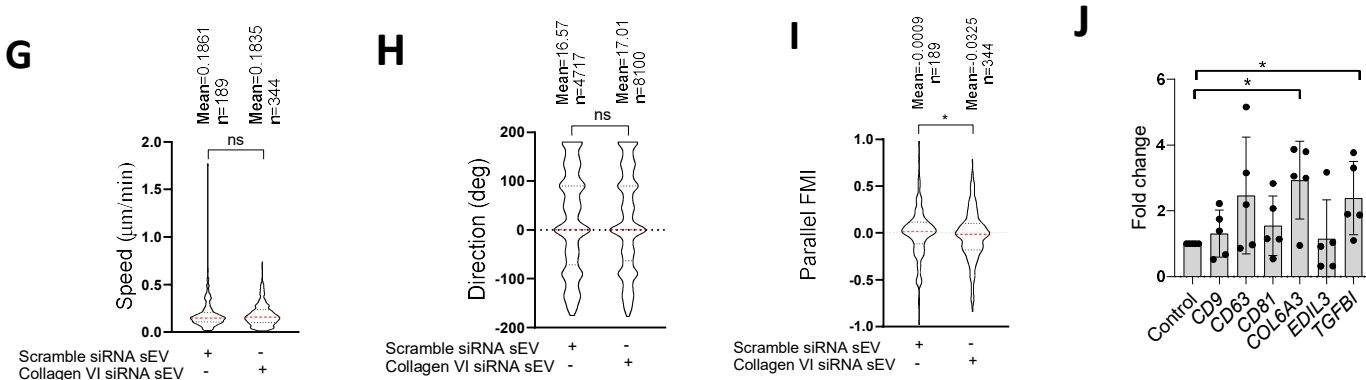
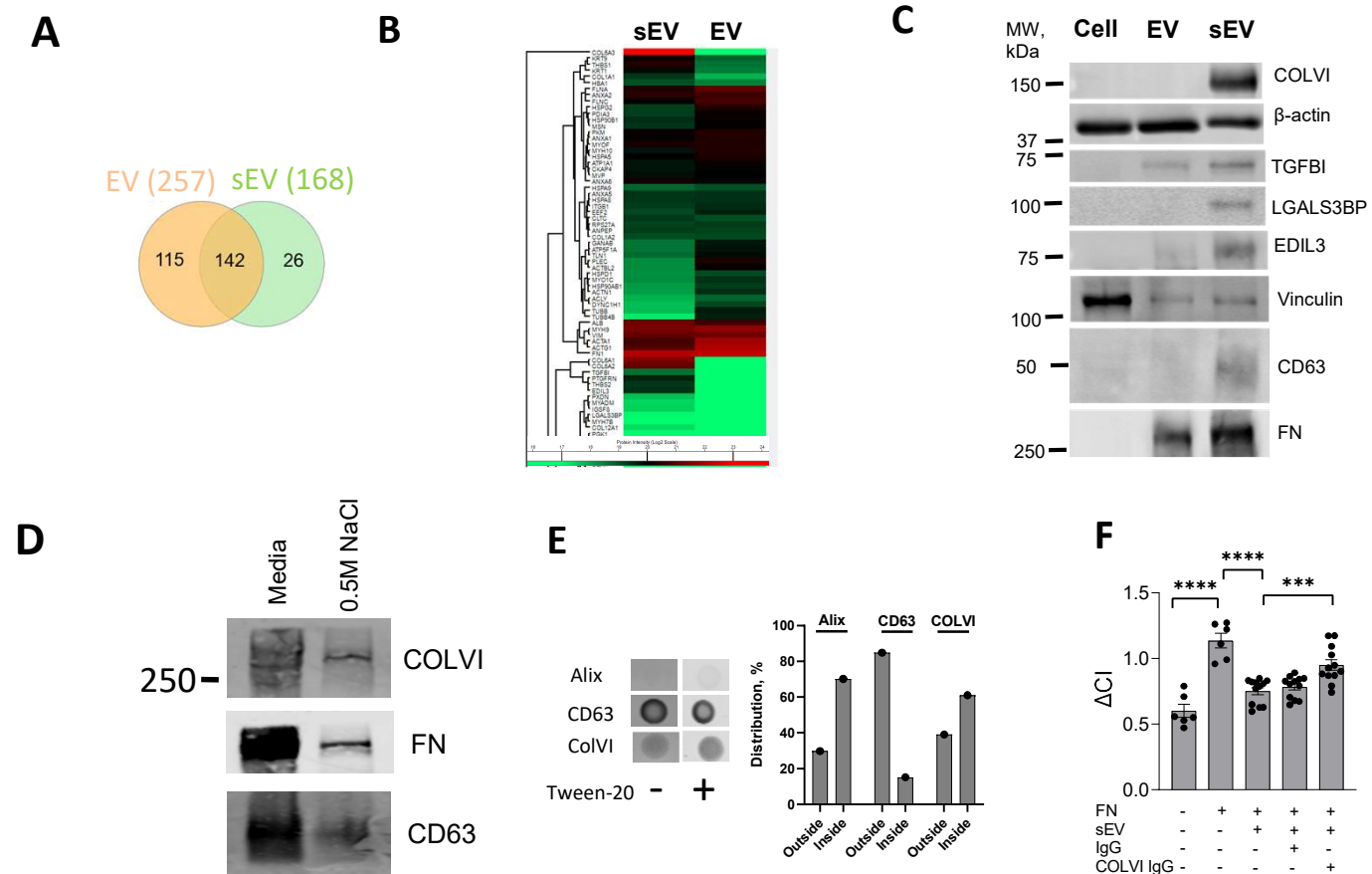


Figure 7. sEVs block focal adhesion formation by presenting collagen VI.

A, Proteomic analysis of VSMC-derived sEVs and EVs. Venn diagram. N=3 biological replicates. **B**, Protein enrichment in the EV and sEV proteome. Heat Map. N=3 biological replicates. **C**, Western blot validation of sEV cargos. EVs and sEVs were isolated from VSMC conditioned media by differential ultracentrifugation and analysed by western blotting. Representative image from N=3 biological replicates. **D**, Collagen VI was presented in sEVs from conditioned media and in ECM-associated sEVs. sEVs were isolated from conditioned media and 0.5M NaCl ECM fraction by differential ultracentrifugation and analysed by western blotting. **E**, Collagen VI is presented on the surface of sEVs. sEVs were analysed by dot-blot in the non-permeabilised (outside) and permeabilised (inside) conditions. Staining intensity was quantified for non-permeabilised (outside) and permeabilised (inside) conditions. Representative from N=2 biological replicates. **F**, VSMC adhesion is regulated by collagen VI loaded on sEV. FN matrices were incubated with sEV and anti-collagen VI antibody (COLVI IgG) or control IgG. Cell adhesion was tracked by using ACEA's xCELLigence Real-Time Cell Analysis. ANOVA, N=3 biological replicates, ***, p<0.001, ****, p<0.0001. **G, H, I**, sEVs promote directional VSMC invasion. VSMCs were treated with control siRNA (Scramble) or collagen VI-specific siRNA pools for 24h and were seeded to the FN-enriched Matrigel matrix in a μ-Slide Chemotaxis assay and stained with Draq5. Cell tracking was conducted by OperaPhenix microscope for 12h and cell invasion parameters were quantified using Columbus, n indicates the total number of tracked cells per condition, Kolmogorov-Smirnov test, *, p<0.05. **I**, Real-time PCR analysis of expression of CD9, CD63, CD81, COL6A3, EDIL3 and TGFBI in atherosclerotic plaque. *, p<0.05, Paired t-test, N=5 patients.

Supplementary Figures

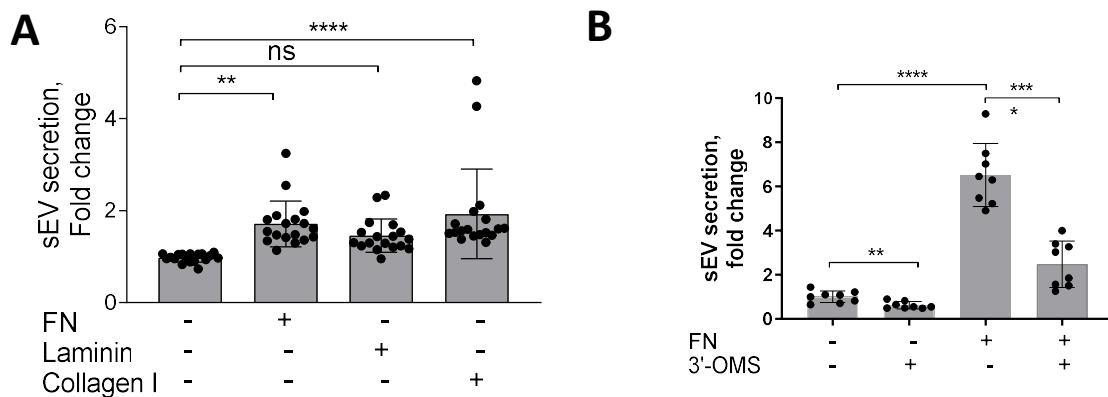


Figure S1. FN matrix stimulates sEV secretion by VSMCs. **A**, FN and collagen I but not laminin stimulate secretion of CD63-enriched sEVs. VSMCs were plated on the various matrices for 24h and sEV secretion was measured by CD63-beads assay. N=3, biological replicates, n=6 technical replicates. ANOVA **p<0.01 **B**, Inhibition of SMPD3 blocks sEV secretion by VSMC plated onto FN matrix. VSMCs were plated on non-coated or FN-coated plates for 24h and conditioned media was analysed by CD63-bead assay. N=2 biological replicates, n=4 technical replicates, ANOVA, ***, p<0.001, ****p<0.0001

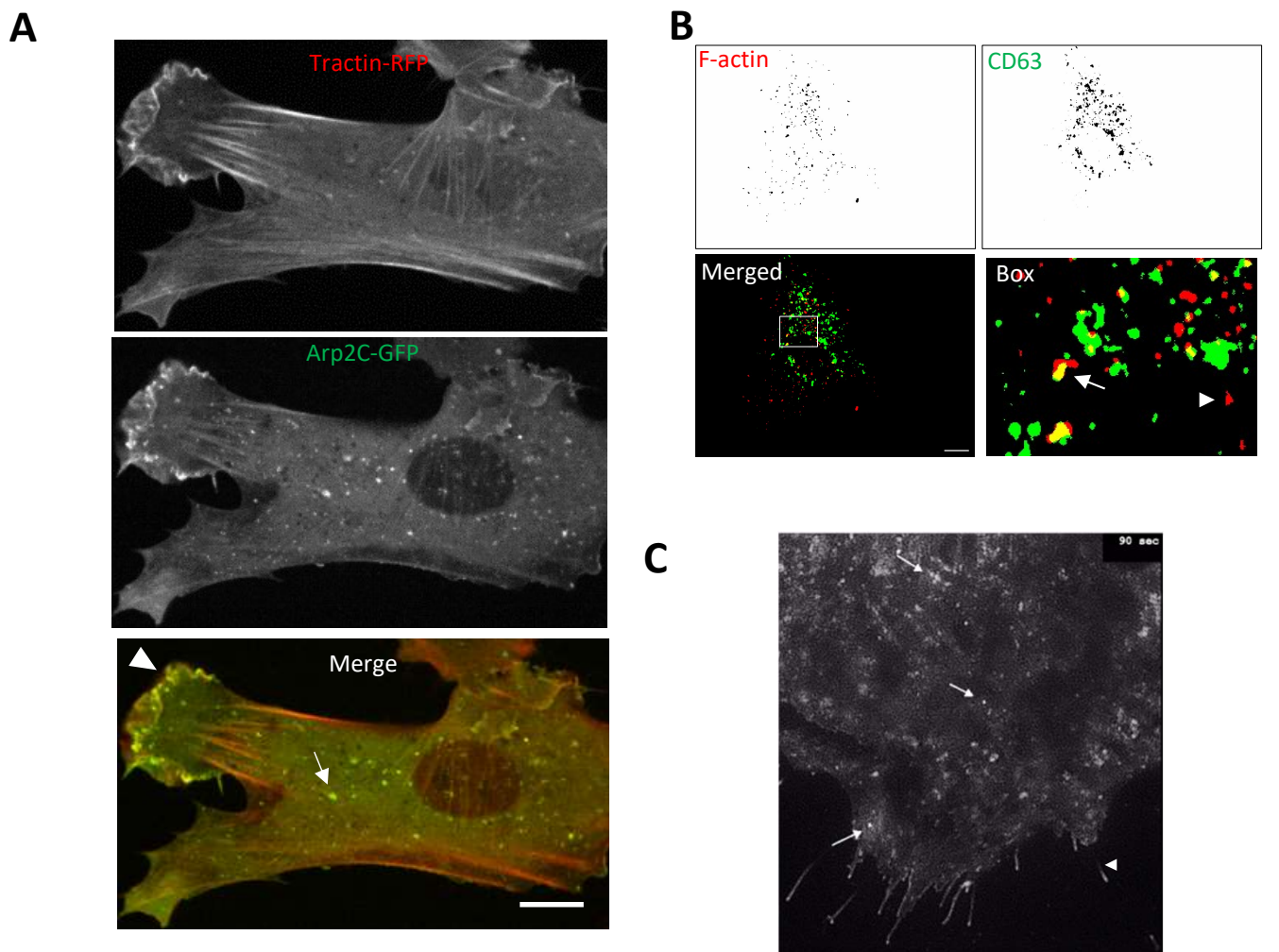


Figure S2. A, Still images of a time-lapse showing that Arp2/3 and F-actin form tails in VSMC cytosol. VSMCs were co-transfected by ARPC2-GFP and F-tractin-RFP and cultured for 24h. Time-lapse video was captured using confocal spinning disk microscopy. Note, that Arp2/3 and F-actin are observed in lamellipodia but also detected in the cytosol with the unknown activity (arrow). Size bar, 10 μ m **B**, Analysis of F-actin/CD63 overlap using ImageJ in a fixed VSMCs. F-actin and CD63 images (Fig 2D) were converted to 8 bits and thresholded. Actin stress fiber structures were extracted from the image by using ParticleAnalysis plug-in (Size (pixel 2) 10-infinity; Circularity 0.5-1) and overlap image created (merged). CD63 endosomes (pseudo coloured in green) were overlapped with F-actin spot-like structures (pseudo coloured in red). Note that endosomes partially overlapped with F-actin tail-like structures (arrows) though some F-actin spots and endosomes were not colocalised (arrowheads).

C, sEV secretion detected with CD63-pHluorin. VSMCs were co-transfected with CD63-pHluorin and incubated for 24h. Time-lapse was captured using confocal spinning-disk microscopy. Arrows, typical “burst”-like appearance of sEV secretion at the cell-ECM interface. Arrows, an intense CD63-pHluorin staining along filopodia-like structures indicating that sEV release can occur in filopodia. Size bar, 10 μ m

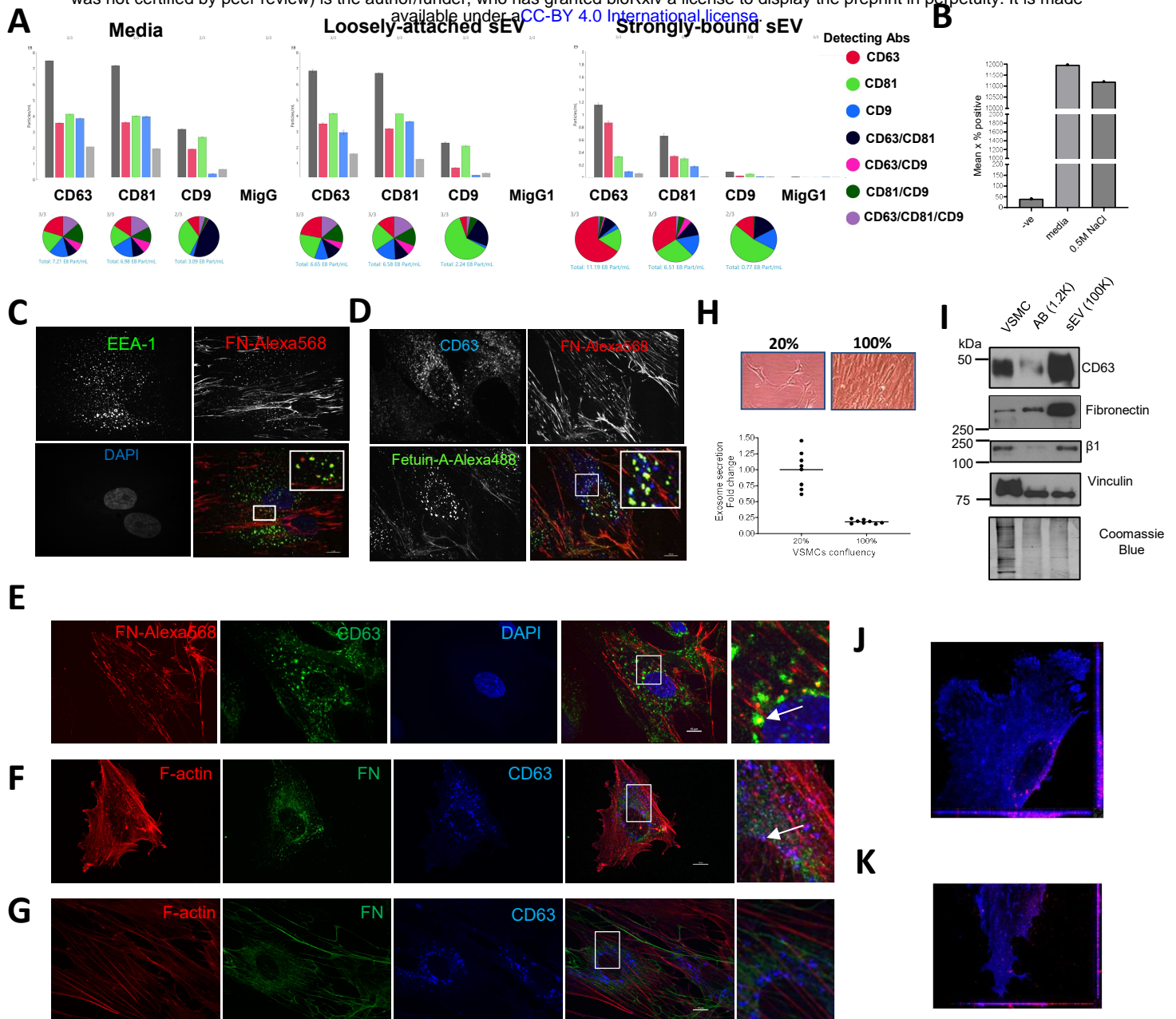


Figure S3 SMPD3-dependent sEVs are trapped in ECM. **A**, Characterisation of sEVs extracted from VSMC-derived media and ECMs fractions. sEVs were sequentially extracted and fractions were collected and analysed by using ExoView. X-axis – capturing spot antibodies (CD63, CD81, CD9 and control MigG1). **B**, CD63-bead capturing assay shows similar enrichment in CD63+/CD81+ sEVs in the conditioned media and ECM-associated sEVs extracted using 0.5M NaCl. VSMCs were plated onto gelatin-covered plates for 10 days and media was collected every 3d. sEVs were extracted in a mild (0.5M NaCl) conditions and media and 0.5M NaCl fractions were analysed by using CD63-beads capturing assay. **C, D**, Exogenously added FN-Alexa568 can be detected in the early endosomes and MVBs. VSMC were serum-deprived for 24h and then incubated with FN-Alexa568 for 30min (C) or 3h (D) in RPMI-0.5% BSA, thoroughly washed and fixed and stained for EEA-1 (C, green) or CD63 (D, blue). Size bar, 10um. **E**, Exogenously added FN-Alexa568 can be detected in MVBs. VSMC were incubated with FN-Alexa568 for 3h and stained for CD63 which was visualised with anti-mouse-Alexa488 antibody. Size bar, 10um, Note the partial colocalization of FN and CD63. **F, G**, FN can be detected in the CD63+ MVBs in a sparsely growing VSMCs. VSMC were plated at low (5,000 cells per well, F) or high density (20,000 cells per well, G) and were cultured for 24h in RMPI supplemented with 2.5% EV-free FBS, fixed and stained for F-actin, FN and CD63. **H**, VSMC plating density influences secretion of CD63+/CD81+ sEVs. Cells were plated at the different density and cultured for 24h and sEVs in conditioned media were measured by CD63-beads assay. N=1 biological replicates, n=8 technical replicates. **I**, FN is presented in sEV along with β 1 integrin. **J**, VSMC were plated on the FN-coated dishes and Alexa568-labelled sEV were added to the cell media for 3h. Cells were fixed and stained for filopodia marker Myo10 (green) and vinculin (blue). Note perinuclear localisation of internalised sEVs. Size bar, 10 μ m. 3D projection. Myo10 staining channel is removed. **K**, VSMC were plated on the FN-coated dishes pre-coated with Alexa568-labelled sEV and incubated for 24h. Cell staining as in Fig S3J. Note even distribution of sEVs across the extracellular matrix and cell area.

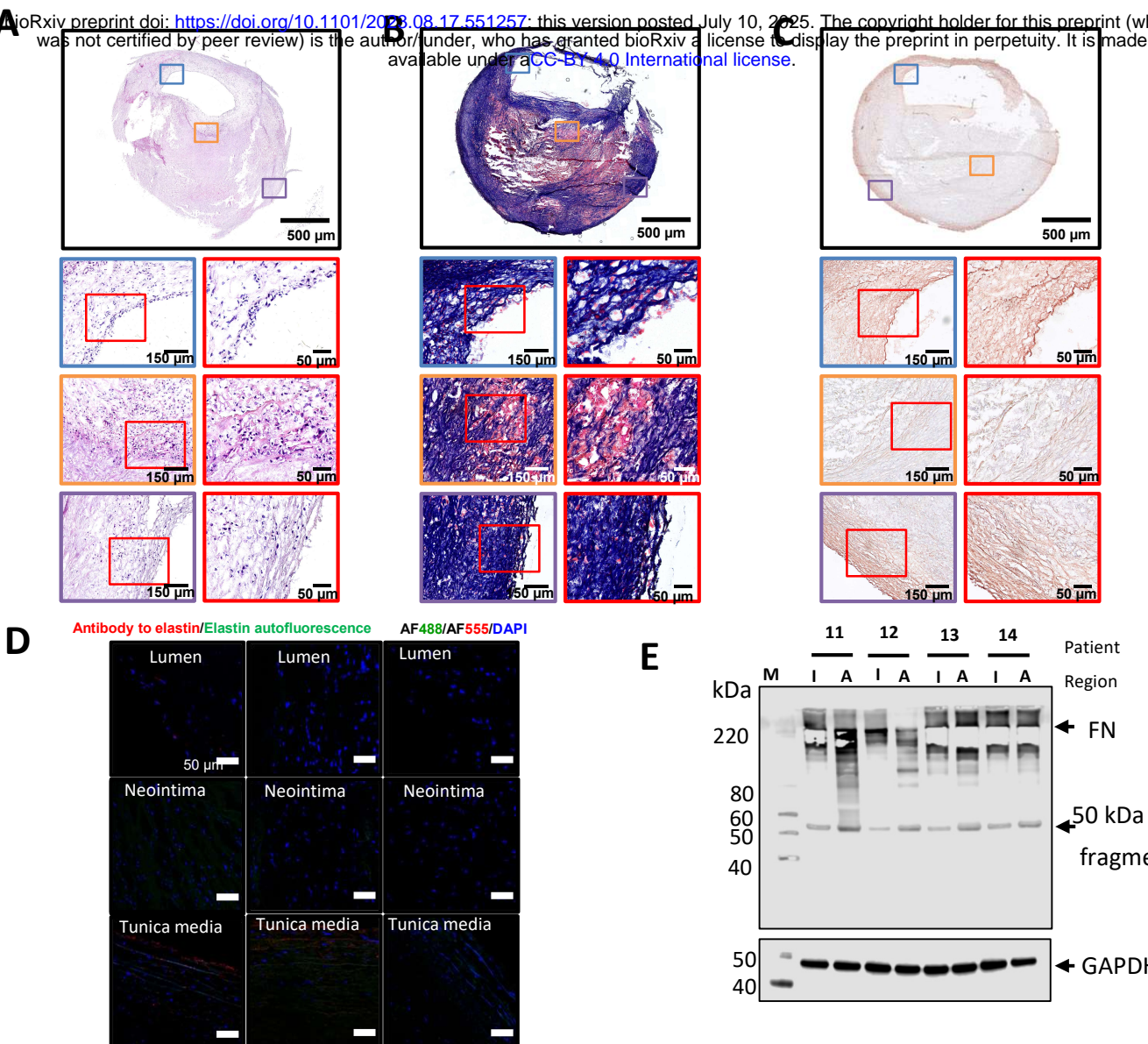
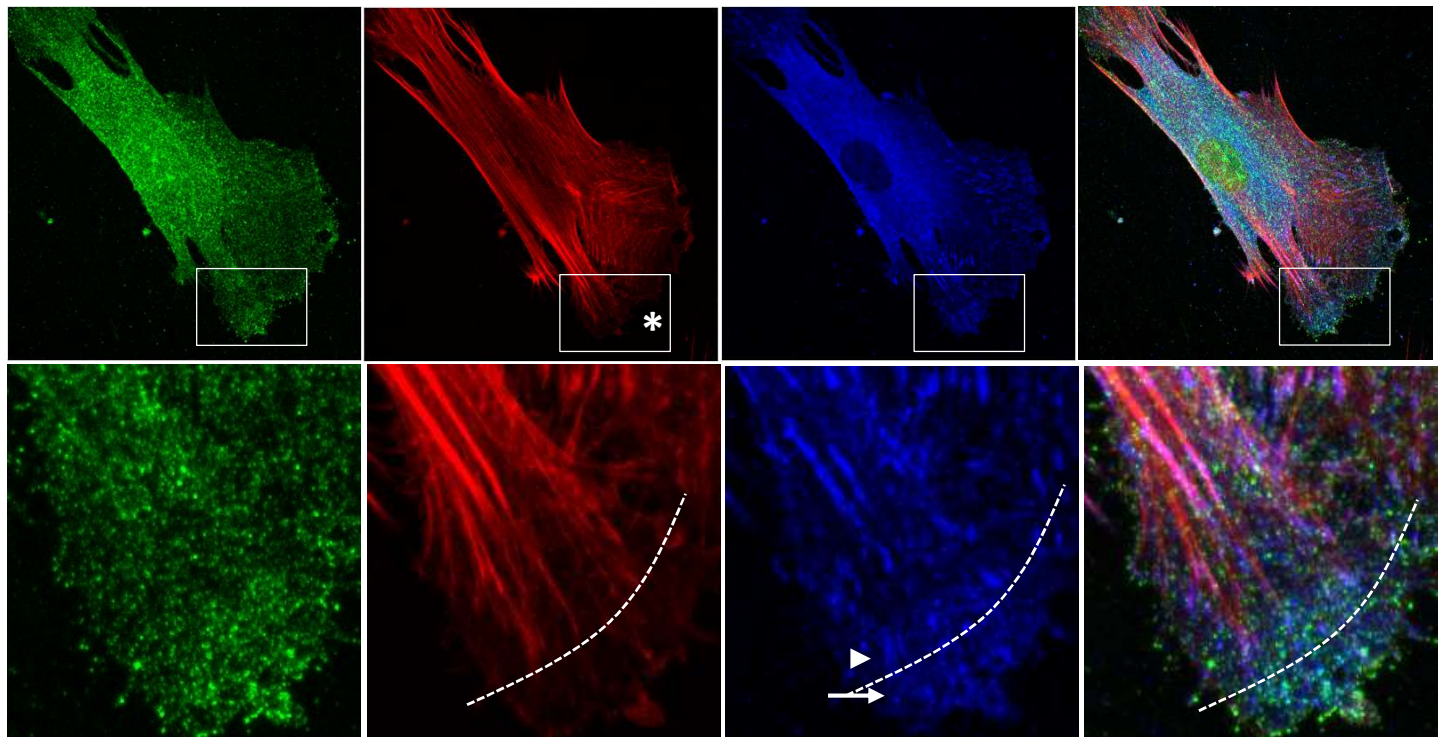


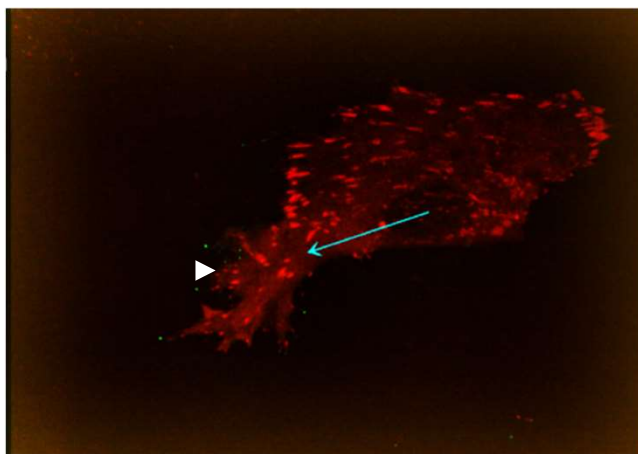
Figure S4. Fibronectin deposition in the atherosclerotic plaque is spatially associated with sEV marker CD81.

A. Staining of atherosclerotic plaques with haematoxylin and eosin. Unstable atheroma with an extracellular lipid or necrotic core and calcification (type IV according to the American Heart Association). Below are representative fields of view focusing on the lumen (blue contour), neointima (green contour), and tunica media (yellow contour). Red contours demarcate representative fields of view within these tissue compartments. Note multiple cells at the luminal side, numerous leukocytes in the neointima, and abundant cells in the tunica media. Overview images: magnification: $\times 1.8$, scale bar: 500 μm ; close-ups demarcated by blue, green, and gold contour: magnification: $\times 200$, scale bar, 150 μm ; close-ups demarcated by red contour: magnification: $\times 400$, scale bar: 50 μm . **B.** Staining of atherosclerotic plaques with Masson's trichrome. Note the superficial erosions at the luminal side, abundant haemorrhages in the neointima, and sporadic haemorrhages in the tunica media. Overview images: magnification: $\times 1.8$, scale bar: 500 μm ; close-ups demarcated by blue, green, and gold contour: magnification: $\times 200$, scale bar: 150 μm ; close-ups demarcated by red contour: magnification: $\times 400$, scale bar, 50 μm . **C.** Staining of atherosclerotic plaques with orcein. Note the moderate connective tissue staining at the luminal side, weak connective tissue staining in the atheroma with a confluent extracellular lipid core, and strong specific staining at the tunica media containing elastic fibres. Overview images: magnification: $\times 1.8$, scale bar: 500 μm ; close-ups demarcated by blue, green, and gold contour: magnification: $\times 200$, scale bar: 150 μm ; close-ups demarcated by red contour: magnification: $\times 400$, scale bar, 50 μm . **D.** Demarcation of tunica media from the neointima using specific antibodies to elastin (red colour) and non-specific autofluorescence of elastic fibers (green colour). Nuclei are counterstained with 4',6-diamidino-2-phenylindole (DAPI, blue colour). Two representative images per each vascular compartment (luminal side, neointima, and tunica media) are provided. Negative controls (i.e., sections stained with species-specific pre-adsorbed fluorescent-labeled secondary antibodies and DAPI but without the respective antigen-specific primary antibody) are provided to the right from representative images. Magnification: $\times 200$, scale bar, 50 μm . Note that elastin is expressed exclusively in the tunica media and is associated with elastic fibers. **E.** Expression of FN in atherosclerotic plaques. Atherosclerotic plaques (A) and adjacent intact arterial segments (I) were homogenised and analysed by Western blotting. FN is abundantly presented in both regions and 50 kDa FN fragment (Homandberg et al., 1992) intensity was used to quantify FN amount.

A



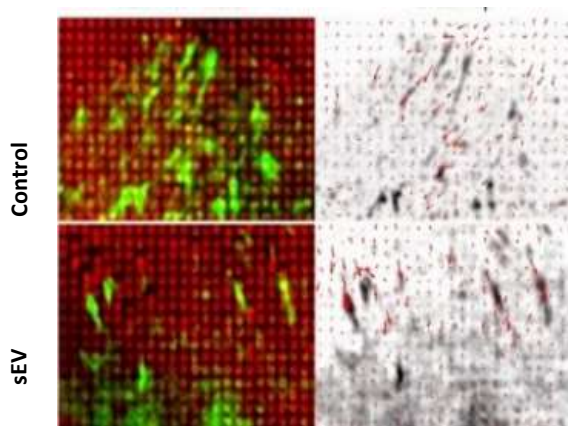
B



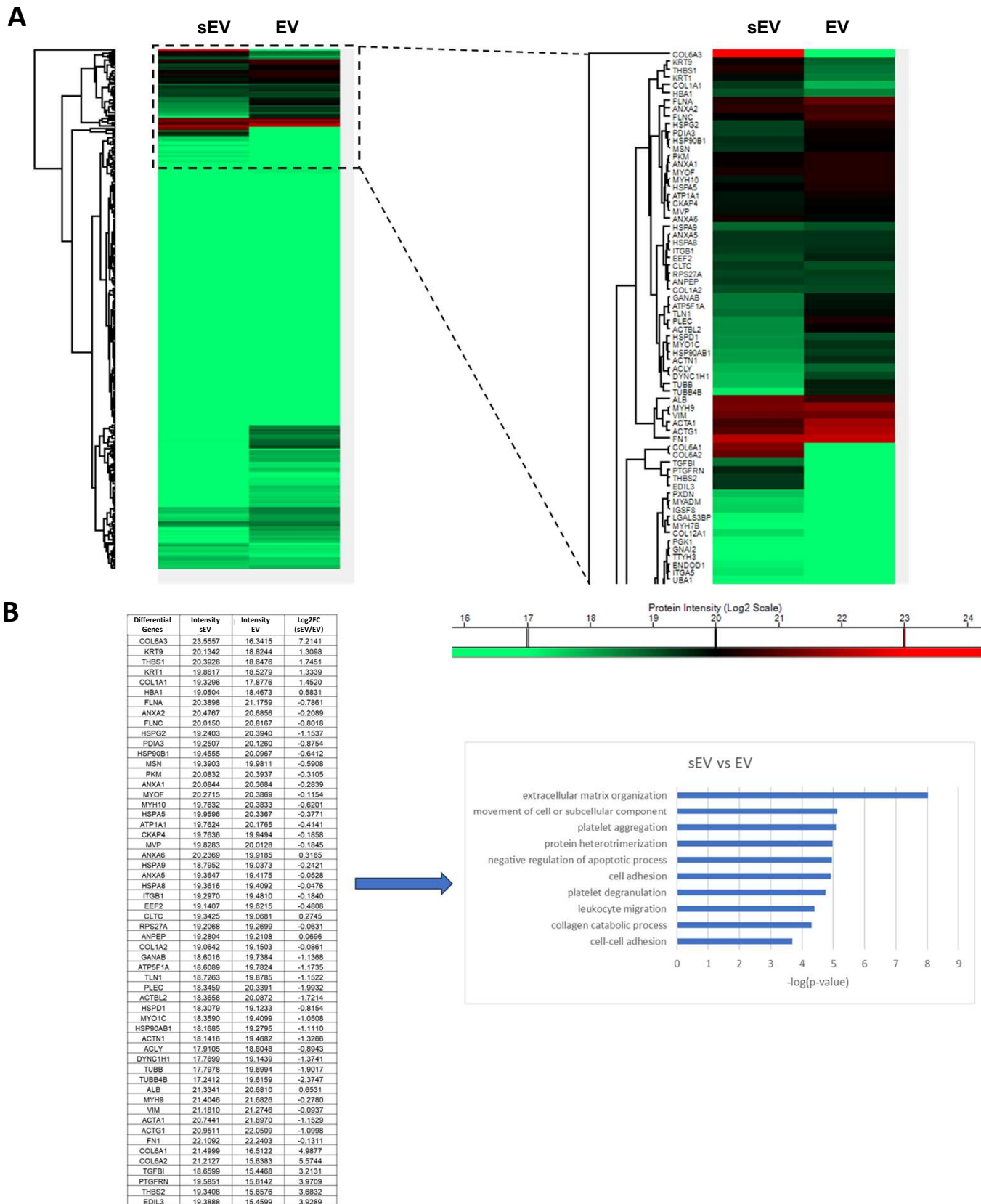
C

Paxillin + Pillars

Forcemap



Supplementary Figure S5 sEVs regulate VSMC motility and invasion. A, Centripetal FAs are linked to actin stress fibers. VSMCs were plated on FN-coated plate for 24h and cells were stained for Myo10 (green), CD63 (blue) and F-actin (phalloidin, red). Note the dot-like focal complexes in lamellipodium which are not associated with the contractile actin bundles (arrow) and an appearance of elongated FAs associated with the mature actin bundles (arrowhead). Dotted line, approximate position of the lamellipodium boundaries. Size bar, 10 μ m. **B**, Mature focal adhesion turnover is not affected by sEVs. VSMC were transfected with Paxillin-RFP and plated on the FN in the absence or presence of immobilised sEVs. Images were captured for 30min using confocal spinning disk microscopy. Note the appearance of the mature FAs in the lamellipodium (Arrowhead). Arrow, direction of the VSMC movement. Representative from N=4 biological replicates. **C**, sEV induces formation of FAs with the enhanced pulling force. VSMC transfected with Paxillin-RFP were plated on the PDMS pillars which were covered with FN and sEVs and pillar displacements were quantified. Representative image from N=2 biological replicates.



Supplementary Figure S6. Proteomic analysis of VSMC-derived sEVs and EV. VSMC-derived EVs and sEVs were isolated from cells and analyzed by protein mass-spectrometry. N=3 biological replicates. **A.** Clustered proteomic heatmap for EV and sEV. **B.** The GO term analysis was performed using the differentially expressed genes between the sEV and EV groups.